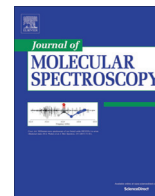




Contents lists available at ScienceDirect

Journal of Molecular Spectroscopy

journal homepage: www.elsevier.com/locate/jms

Line shape parameters of air-broadened water vapor transitions in the ν_1 and ν_3 spectral region

V. Malathy Devi^{a,*}, Robert R. Gamache^b, Bastien Vispoel^b, Candice L. Renaud^b, D. Chris Benner^a, Mary Ann H. Smith^c, Thomas A. Blake^d, Robert L. Sams^d

^a Department of Physics, College of William and Mary, Williamsburg, VA, USA

^b Department of Environmental, Earth, and Atmospheric Sciences, University of Massachusetts Lowell, Lowell, MA, USA

^c Science Directorate, NASA Langley Research Center, Hampton, VA, USA

^d Pacific Northwest National Laboratory, Mail stop K4-13, Battelle Boulevard, P.O. Box 999, Richland, WA, USA

ARTICLE INFO

Article history:

Received 25 August 2017

In revised form 17 October 2017

Accepted 21 November 2017

Available online xxx

Keywords:

H₂O

Spectral line shapes

Air-broadening

Temperature dependence of line shapes

Relaxation matrix element coefficients

Speed dependence

ABSTRACT

A Bruker IFS-120HR Fourier transform spectrometer located at the Pacific Northwest National Laboratory (PNNL) in Richland, Washington was used to record a series of spectra of pure H₂O and air-broadened H₂O in the regions of the ν_1 and ν_3 bands (3450–4000 cm⁻¹) at different pressures, temperatures and volume mixing ratios of H₂O in air. Eighteen high-resolution, high signal-to-noise (S/N) ratio absorption spectra were recorded at T = 268, 296 and 353 K using two temperature-controlled absorption cells with path lengths of 9.906(1) and 19.95(1) cm. The resolution of the spectra recorded with the 9.906 cm and 19.95 cm absorption cells was 0.006 and 0.008 cm⁻¹, respectively. A multispectrum nonlinear least squares fitting technique was employed to fit all the eighteen spectra simultaneously to retrieve 313 accurate line positions, 315 intensities, 229 Lorentz air-broadened half-width and 213 air-shift coefficients and their temperature dependences (136 for air-broadened width and 128 for air-shift coefficients, respectively). Room temperature self-broadened half-width coefficients for 209 transitions and self-shift coefficients for 106 transitions were also measured. Line mixing coefficients were experimentally determined for isolated sets of 10 transition pairs for H₂O-air and 8 transition pairs for H₂O-H₂O using the off-diagonal relaxation matrix element formalism, and 85 quadratic speed dependence parameters were measured. Modified Complex Robert-Bonamy (MCRB) calculations of self-, and air-broadened (from N₂- and O₂-broadening) half-width and air-shift coefficients, and temperature dependence exponents of air-broadened half-width coefficients are made. The measurements and calculations are compared with each other and with similar parameters reported in the literature.

© 2017 Elsevier Inc. All rights reserved.

1. Introduction

Accurate knowledge of spectroscopic line parameters for all atmospheric molecules, particularly for water vapor transitions is not only of great importance but also crucial for reliable remote sensing applications for Earth's and other planetary atmospheres (e.g., Mars), exoplanets, comets, brown dwarfs and stellar atmospheres, e.g. [1–6]. H₂O is one of the most important and ubiquitous atmospheric molecules whose line parameters are listed first in well-known spectroscopic databases such as HITRAN and GEISA [1–3]. Because of its importance in many spectroscopic applications, its spectrum has been the subject of numerous

experimental and theoretical investigations (e.g. [6–35] and other references therein). The water molecule has nine isotopologues (H₂¹⁶O, H₂¹⁷O, H₂¹⁸O, HD¹⁶O, HD¹⁷O, HD¹⁸O, D₂¹⁶O, D₂¹⁷O, and D₂¹⁸O) and each has three fundamental vibrational bands, ν_1 , ν_2 and ν_3 . However, there are a very large number of overtone, combination, and difference bands arising from these three fundamental vibrations, and the reader may refer to Refs. [1–3] for a general idea of the enormous number of water vapor transitions and the numerous spectroscopic investigations (e.g., [7–35]) performed on the various water vapor bands. In 2004, Barber et al. [6] reported the (then) most complete calculated water vapor line list comprising more than 500 million transitions, and commented that over 90 percent of all known experimental water vapor energy levels (at that time) agreed within 0.3 cm⁻¹ of their calculated values. Line parameter measurements for the fundamental bands, and a number of overtone, combination and difference bands of water

* Corresponding author at: Department of Physics, The College of William and Mary, Williamsburg, VA 23187-8795, USA.

E-mail address: malathy.d.venkataraman@nasa.gov (V. Malathy Devi).

vapor using high-resolution instruments have been reported by numerous investigators over the past several decades, and the number of experimental and theoretical studies related to the research available in the literature is huge. Therefore, the references listed in this work are in no way considered exhaustive because only limited studies that are most relevant to the present measurements are cited in this work.

At low gas sample pressures, the basic parameters needed to characterize any molecular band transitions are their line positions and line intensities. At higher sample pressures, information on line width and line shift coefficients become important. Depending upon the sample gas mixtures and their temperatures, additional information such as self-broadened and foreign-gas broadened (e.g., air, N₂, O₂) half-width coefficients and the corresponding line shift (pressure-shift) coefficients and their variations as a function of sample gas temperature must be known for proper characterization of any specific band. When spectra are obtained at relatively high resolution and high S/N ratios, depending on the applications that are sought, knowledge of sophisticated and detailed line shape parameters such as the line narrowing (Dicke narrowing), line mixing (first order Rosenkranz approximation or full relaxation matrix element formalism), speed dependences of Lorentz broadening and pressure-shift coefficients, and their variations with temperature also become important, and are required for applications such as accurate remote sensing measurements.

Different analysis techniques are employed by various investigators to retrieve the spectroscopic information from the recorded spectra. In some studies, line parameters are determined by analyzing small spectral intervals (micro-windows) involving line-by-line and spectrum-by-spectrum fittings in all of the recorded spectra followed by computing the average of many such measurement results; while in other studies larger spectral intervals (extending from a few to several tens of cm⁻¹ wide) from a number of spectra are simultaneously fitted to obtain a unique and self-consistent set of line parameters. In other instances, the entire molecular band could be fitted all at once for several spectra obtained at various experimental conditions of temperature and pressure, simultaneously. From the analysis point of view, some spectrum fitting software could provide an extensive error analysis of the retrieved line parameters. When several research groups report measurements of certain specific line parameters (e.g., position, intensity) for a ro-vibrational band, comparisons of measurements are expected irrespective of the quality of data to be compared with. In some cases, very good/excellent agreement among different measurement sets is observed and, at other times the agreement with other studies may be found to be poor. It should be noted that in order to compare values among different sets of measurements it is imperative that the quality of data analyzed and the software used to retrieve the data must be similar. It is not always possible to achieve such standardization among different laboratory studies, however, including the present study (PS) with measurements from other laboratories.

A literature survey shows that there have been a large number of high-resolution measurements of line shape parameters using different broadening gases for the various water vapor bands employing several measurement techniques (e.g., [7–28]). For analyzing remotely sensed terrestrial atmospheric spectra, particularly stratospheric spectra, air-broadened line shape parameters (such as pressure-broadened widths, shifts, and their temperature dependences) are more important and necessary than the self-broadening parameters. However, because of the roughly five times larger self-broadened half-width coefficients compared to the corresponding air-broadened half-width coefficients, information on self-broadened line shape parameters also becomes important. As pointed out by Brown et al. [36] in the case of methane, which is also true for all other molecules including water, one of

the major shortfalls in the knowledge of line parameters is the large uncertainties for the pressure-broadened line shape parameters throughout the databases [1–3]. It is apparent from the results available for water vapor transitions of the fundamental bands, that the majority of the studies related to line shape parameters for common broadening gases (such as self, air, N₂, O₂) concern mostly the ν_2 band. This has been particularly true for the air-broadening measurements until recently. The first (and only) laboratory measurements of line mixing in H₂O were also carried out in the ν_2 band [19]. The major objectives of the present study therefore, were to measure air-broadened half-widths, pressure-shifts and their temperature dependences, and to determine line mixing parameters where possible, for transitions in the ν_1 and ν_3 bands.

In this study, we report measurements of line positions, intensities, air-broadened half-width and pressure-shift coefficients and their temperature dependences for the strong transitions in the ν_1 and ν_3 bands of H₂¹⁶O in the 3645–3980 cm⁻¹ range. Room-temperature measurements of self-width and self-shift coefficients were also obtained for a number of strong transitions. When the present study was just completed and the manuscript was in preparation, new results of self-broadened [26] and air- and self-broadened line shape parameters were reported [27,28]. The measurements by Ptashnik et al. [26] on self-broadening were published in late 2016. The recent results of Loos et al. [27,28] include more transitions than the present results because of the larger absorption path lengths available in Refs. [27,28]. The present results are compared and contrasted with those listed in Refs. [27,28] along with some other measurements from Refs. [15,26].

A list of all measured line parameters along with the calculated values using the Modified Complex Robert-Bonamy (MCRB) formalism will be provided as a [Supplemental file](#) available in the online version of this article.

2. Experimental details

The Bruker IFS-120HR Fourier transform spectrometer (FTS) at the Pacific Northwest National Laboratory (PNNL) located in Richland, Washington was used to record the spectra for the present analysis. Two absorption cells with path lengths of 9.906(1) and 19.95(1) cm were used to contain the gas samples. A total of eighteen spectra (seven pure H₂O and eleven air-broadened H₂O) were recorded at temperatures T = 268, 296 and 353 K. Sixteen of those spectra were obtained at 0.008 cm⁻¹ resolution using the 19.95 cm cell, while the remaining two pure H₂O spectra were recorded at 0.006 cm⁻¹ resolution using the 9.906 cm path cell. Both of these specially built absorption cells were made of stainless steel, electroplated and gold-coated to minimize decomposition and sticking of the gas samples and, to minimize reactivity when using corrosive gases such as HCN. Both cells have an inner diameter of 5 cm. The two cells are coolable to ~215 K and can also be heated to 373 K.

For the present measurements, the entire spectrometer bench and the sample compartment were kept under vacuum (below 0.03 Torr) using a mechanical vacuum pump. A ½" diameter copper tube, positioned horizontally, ran the length of the moving mirror compartment, and both ends of the tube came out of the spectrometer through vacuum feed-through fittings. The ends of the tube were bent so they were vertical. This tube was kept filled with liquid nitrogen for the duration of each measurement. Two molecular sieve sorption traps were connected to the sample and detector vacuum chambers, and these traps were cooled to liquid nitrogen temperature during the duration of each measurement. The spectra using the 9.906 cm and the 19.95 cm cells were obtained during two different experimental setups which were several months apart, and slightly different spectral resolutions were used in

acquiring the data. In each experimental setup, the absorption cell was mounted inside the sample compartment of the spectrometer to avoid errors associated with beam steering due to cell misalignment. A temperature-regulated water jacket surrounds this inner tube and is plumbed through the spectrometer's vacuum bulkhead to a circulating water bath (Julabo F25-MD). The cell is actively temperature stabilized by either heating or cooling the circulating fluid, which consists of a weak solution of propylene glycol in water. A single RTD sensor was used to monitor the temperature of the sample cell and hence the gas mixtures. The cell is connected to the sample manifold via a valve located inside the spectrometer to minimize dead volume. This valve in turn is plumbed through the spectrometer's vacuum bulkhead to a manifold, which has numerous valved ports for pumping and sample introduction. Three precision Baratrons (MKS-690A) with full range pressure measurements of 0–1, 0–10 and 0–1000 Torr and accuracies of $\pm 0.05\%$ of the pressure reading are coupled to the manifold through short sections of tubing. Pressures in the sample cells were measured using the one of the three manometers that gave the most accurate reading for the sample pressure range. A diffusion pump is used to evacuate the manifold and the gas cell. Sample fillings and nitrogen backfilling of the sample are automated by computer control of the manifold and associated valving.

The 19.95 cm cell was fitted with 2-in diameter wedged KCl windows sealed against the cell using Viton O-rings. The shorter 9.906 cm long cell used wedged BaF₂ windows also sealed to the ends of the cell with Viton O-rings. Although a number of higher pressure and heated self-broadened H₂O spectra were recorded using this cell, those spectra were not included in the present analysis. Hence it was not possible to extract information of temperature dependences of self-broadened line shape parameters from the dataset used in this study. The gas sample temperatures are known to ± 0.02 K or better in both experiments. Spectra were recorded using a CaF₂ beam splitter and an InSb detector. Digital filters set for the spectral region of interest were used to minimize the size of the interferograms. For each background or sample spectrum recorded, either 128, 256, 384 or 512 single-sided interferograms were co-added. For Fourier transform conversion, a Mertz-phase correction, 1 cm⁻¹ phase resolution, zero-filling factor of 2, and box car apodization were applied to the averaged interferograms. The signal-to-noise ratios of the recorded spectra were >1500, dependent on the number of co-added scans. Additional details of the experimental setup with the 19.95 cm cell are available in Refs. [37,38].

Appropriate precautions were taken to condition the absorption cells for the pure water vapor and H₂O-air gas mixtures to attain equilibrium pressure and temperature conditions before the data recordings were started. Water samples were purified before introducing into the absorption cell to remove impurities such as air and CO₂. With the 19.95 cm cell, for each air-broadened spectrum the H₂O was introduced into the cell first, followed by the research grade synthetic air. After recording each spectrum, the cell and connecting tubing to the manifold were thoroughly pumped down, backfilled with dry nitrogen gas and pumped again before a new sample was introduced into the absorption cell. The self-broadened H₂O spectra with the 19.95 cm cell were recorded the day after all of the air-broadened spectra were completed, allowing the cell to pump down overnight between the two series, and the self-broadened H₂O spectra with the 9.906 cm cell were recorded several months later, using similar filling and pumping procedures. In the recorded spectra, no CO₂ lines were observed (in the 3500–3750 cm⁻¹ region). The wavenumber range of all spectra was limited to 2950–4947 cm⁻¹.

Since our main goal was to examine temperature dependences of line widths and shifts (and possibly detect line mixing) for the strongest transitions in the ν_1 and ν_3 bands, the optical density of

spectra used in the present dataset was not high; thus, the absorption features corresponding to high- J transitions were weak, and only a very few $2\nu_2$ lines were measured in this work. Several background empty-cell spectra were recorded in order to compute ratio spectra which were used in the analysis. Calibration of wavelength scales of the spectra was achieved using the accurate positions of the CO 2 ← 0 lines [39].

Although wedged windows were used in the absorption cells, channel spectra were still present in the recorded spectra. Two channel spectra were observed in the two low-pressure pure water vapor data recorded with the shorter cell, while three channel spectra appeared in the 19.95 cm data. The amplitude and phase of these channelings changed slightly with wavenumber while the periods of the channel spectra were nearly the same. As a result, small residual channelings were present even in the ratio spectra. The channel spectra were more prominent in the low-pressure pure H₂O spectra and were minimal in the air-broadened spectra. The amplitudes of the residual channelings were between ± 0.002 and they did not appear to affect the 100% absorption level.

2.1. Sample spectra

Compressed plots of a few spectra analyzed in this study are illustrated in Fig. 1 where laboratory absorption spectra of one pure H₂O (top panel a) at 296 K, and three air-broadened H₂O spectra recorded at 296 K, 268 K and 353 K are shown in panels (b)–(d), respectively. The 19.95 cm cell was used for obtaining these spectra and the resolution of the spectra was set to 0.008 cm⁻¹. On the 0 → 1 range chosen for the y-axis scale in Fig. 1, no channeling is apparent in the pure sample spectrum. Brief experimental conditions of the spectra are given in the appropriate figure legends and more details are listed in Table 1.

Examples of channel spectra (3717–3729 cm⁻¹) observed in two low-pressure pure water vapor spectra recorded with the 19.95 cm cell (see Table 1) are displayed in Fig. 2. Two to three channel spectra (depending upon the absorption path lengths) were observed and fitted satisfactorily (during the analysis) in the appropriate spectra by proper choice of each channel spectrum's amplitude, period and phase. In panels (a) and (c) the two observed low-pressure pure water vapor spectra exhibiting channelings and in (b) and (d) the corresponding weighted fit residuals (observed minus calculated) with channel spectra mostly removed from the data, are displayed. The amplitude and period of the three channel spectra seen in Fig. 2(a) and (c) were 0.00168, 0.00154 and -0.00126 and, 1.195, 0.560 and 0.576 cm⁻¹, respectively for the spectrum in (a) and the corresponding values for the spectrum in (c) were 0.00175, -0.00168 and -0.00118 and, 1.198, 0.560, and 0.577 cm⁻¹, respectively. These channel spectra were mostly eliminated in the fitted ratio spectra as seen in the small uniform residuals plotted in panels (b) and (d). To see details of these channelings, the vertical axes in (a) and (c) are expanded to show only the top 5% of the spectra. The residuals plotted in panels (b) and (d) result from fitting all 18 spectra (Table 1) simultaneously. The characteristics (amplitude, period and phases) of these channel spectra varied slightly with wavenumber and required solving for their values in each fitted region.

3. Multispectrum fitting

3.1. General description of spectrum fittings

The first step prior to starting the multispectrum fitting was to calibrate the wavelength scales of all the spectra such that the line positions in each spectrum to be fitted are aligned properly. This

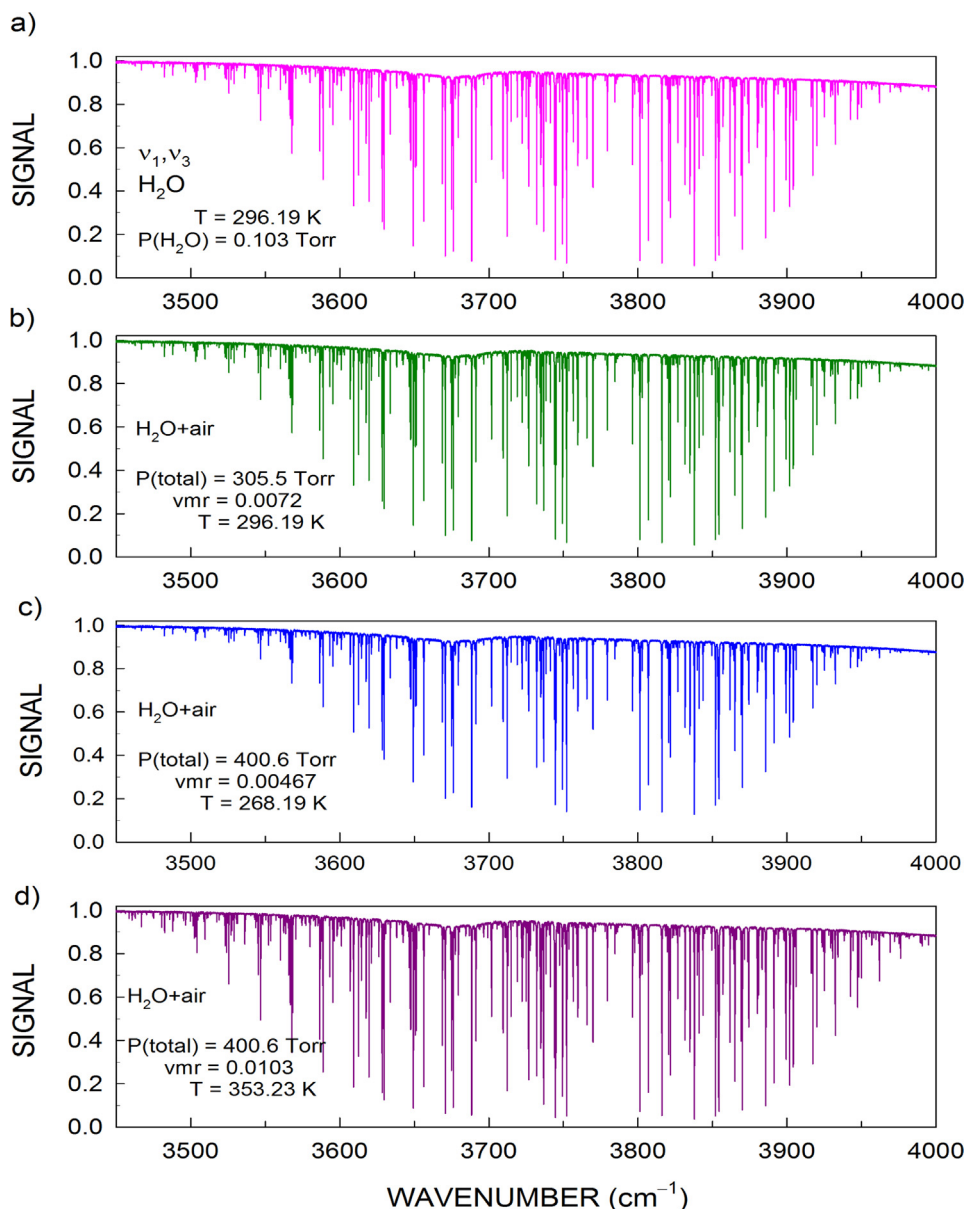


Fig. 1. Compressed plots of a few sample absorption spectra of pure and air-broadened water vapor in the v_1 and v_3 bands between 3450 and 4000 cm^{-1} . The spectra were recorded with the Bruker IFS-120HR FTS at the Pacific Northwest National Laboratory in Richland, Washington. The spectral resolution is 0.008 cm^{-1} and the path length of the absorption cell is 19.95 cm. Brief experimental conditions of the spectra are given in the figure legends in panels (a)–(d) and more details in Table 1.

process was achieved using the accurate positions of the $2 \leftarrow 0$ band lines of CO [39]. A multispectrum nonlinear least squares fitting technique [40,41] was employed to fit all 18 spectra (Table 1) simultaneously. The entire spectral region, extending from 3645 to 3980 cm^{-1} , was covered (except for the short spectral region from 3659 to 3667 cm^{-1} where no major absorption features were observed) by fitting 19 intervals, each ranging between 12 and 24 cm^{-1} wide. The initial line list used for the least squares fittings was taken from the HITRAN2012 database [2]. Since purified (removing contaminants such as trapped air/ CO_2) water vapor samples of natural abundance were used in the experiments, the distribution of the various isotopologue abundances listed in the HITRAN database was used. All spectral lines listed in the HITRAN2012 database were selected with no intensity cutoff to be included in the least squares solution.

The multispectrum analysis was applied interactively. Since no pure water vapor spectra other than at room temperature were recorded, it was not possible to determine accurately the temperature dependences of self-width and self-shift coefficients. Hence the temperature dependences of self-width and self-shift coefficients were fixed to nominal default values of 0.65 and 0.0 $\text{cm}^{-1} \text{atm}^{-1} \text{K}^{-1}$, respectively. The self-width coefficients for weak lines that could not be measured reliably were fixed to the HITRAN2012 values while the self-shift coefficients were fixed to $-0.005 \text{ cm}^{-1} \text{atm}^{-1}$ at 296 K, close to the mean value observed for stronger lines in this spectral region. Similarly, for the weak transitions, air-broadened half-width coefficients, their temperature dependence exponents and air-shift coefficients were fixed to values listed in the HITRAN2012 database. For medium-strength transitions where air-shift coefficients could be measured but not their temperature

Table 1Summary of the experimental conditions of H₂O and H₂O-air spectra analyzed. Path lengths of cells = 19.95 cm^a and 9.906 cm^b.

Serial #	Spectrum file name ^c	Total gas pressure ^d (Torr)	Sample gas temperature ^e (K)	Volume mixing ratio of H ₂ O
<i>Only H₂O</i>				
1 ^a	3450x1393.aus	0.130	296.20	1.0
2 ^a	3450x1397.aus	0.103	296.19	1.0
3 ^a	3450x1394.aus	0.0235	296.20	1.0
4 ^a	3450x1395.aus	0.0690	296.20	1.0
5 ^a	3450x1396.aus	0.0415	296.21	1.0
6 ^b	3450x1609.aus	2.032	298.00	1.0
7 ^b	3450x1612.aus	4.16	298.00	1.0
<i>H₂O + air^f</i>				
8 ^a	3450x1391.aus	150.1	296.20	0.0051
9 ^a	3450x1390.aus	305.5	296.19	0.0072
10 ^a	3450x1389.aus	450.4	296.20	0.00564
11 ^a	3450x1384.aus	100.5	268.20	0.00606
12 ^a	3450x1383.aus	252.7	268.19	0.00438
13 ^a	3450x1382.aus	400.6	268.19	0.00467
14 ^a	3450x1381.aus	600.0	268.19	0.00376
15 ^a	3450x1377.aus	100.8	353.23	0.00775
16 ^a	3450x1376.aus	250.3	353.23	0.00682
17 ^a	3450x1375.aus	400.6	353.23	0.01026
18 ^a	3450x1374.aus	612.9	353.24	0.0200

1 atm = 101.3 kPa = 760 Torr.

^{a,b} Cell length is known with an uncertainty of 0.01% (see the text for details).^c Included for authors' identification of spectra analyzed.^d Gas sample pressures are measured with uncertainties of $\pm 0.05\%$ of full-scale readings of the pressure gauges (1, 10 or 1000 Torr, as appropriate).^e Cell (gas sample) temperatures are measured with uncertainties of ± 0.02 K.^f Research grade air sample was used for the air-broadened H₂O spectra.

dependences, their temperature dependences were fixed to 0.0 cm⁻¹ atm⁻¹ K⁻¹. To minimize the instrumental line shape distortions, the effective apodization factor, residual phase error and the field of view (FOV) corrections were adjusted during the least squares iterations, if warranted.

Collisional line mixing coefficients for H₂O-air and H₂O-H₂O systems were retrieved for specific transition pairs by applying the off-diagonal relaxation matrix element formalism of Levy et al. [42]. A quadratic speed dependence parameter for Lorentz broadened half-width coefficients (a value common for both self- and air-broadening in the present study) was measured where appropriate.

A sample multispectrum fit of all eighteen spectra is displayed in Fig. 3. The set consists of seven pure and eleven air-broadened water vapor spectra between 3830 and 3847 cm⁻¹. The 18 experimental spectra fitted simultaneously are overlaid and plotted vs. wavenumber (cm⁻¹) in (a) and the corresponding weighted (observed minus calculated) fit residuals are shown as a function of wavenumber (cm⁻¹) of the fitted region in panels (b)–(e) for selected spectra grouped together based on their temperature ranges. Although plotted in different panels, the fit residuals in each panel were from the same multispectrum fit. These residuals demonstrate that each of the 18 spectra are fitted to the noise levels of the spectra. Spectra were given weights based upon the quality of each spectrum, a maximum weight of one was assigned to the best spectrum or several spectra of similar high quality. Different colors are used to distinguish the various sets of residuals plotted and the colors of each group of residuals correspond to those in panel (a). The solid horizontal line plotted along the peaks of absorption features in (a) represents the 100% absorption level. The short black lines at the top of panel (a) correspond to positions of lines included in the multispectrum fit. Experimental conditions of all spectra are available in Table 1. There are 170 transitions included in this fitted interval. A Voigt line shape profile with a quadratic speed dependence of Lorentz broadening was employed. In panel (f) the residuals from all spectra with speed dependence removed from the fit are shown which clearly indicate the need to include speed dependence in the solution.

3.2. Line parameters and number of measurements

Since the optical densities of the fitted spectra were relatively small, especially for the pure H₂O spectra, the majority of the transitions measured were from the ν_3 band while a smaller number of transitions from the weaker ν_1 band were observed and measurements were made. A few weak transitions of the $2\nu_2$ and $\nu_2 + \nu_3 - \nu_2$ bands were observed in the fitted regions, but due to their weakness, the accuracies in their measured positions and intensities were poor. Line shape parameters could be obtained for only one transition for the $2\nu_2$ and none for the $\nu_2 + \nu_3 - \nu_2$ band.

The types of line parameters and numbers of measurements made for the each type are listed in Table 2. The first and the third columns list the spectral line parameters while the numbers of measured parameters are listed under the second and the fourth columns. Line intensities of 315 transitions in the whole fitted region were measured, but the line positions were measured for 313 lines because a few lines were either very weak or blended, and the individual positions could not be measured well. It is clear from this table that more parameter measurements were obtained for the air-broadening than for self-broadening. The number of half-widths and pressure-shift coefficients for which temperature dependences were measured is less than the corresponding number of room-temperature measurements. In cases where two components of a collision-mixed transition pair were involved in line mixing, some of their line shape parameters, such as widths, shifts and temperature dependence exponents, were constrained to be the same for both line-mixed components. A quadratic speed dependence (S_4) parameter [43] was included for the majority of the strong transitions; for weak transitions, the speed dependence was fixed to a default value of 0.1 based upon similar measurements on the recent studies of CO₂-broadened HDO transitions (e.g., [44–46]). As in our previous studies [44–46], for doublet transitions whose positions were separated by small amounts, auxiliary parameters were applied to constrain the separation between the lines and their relative intensities. More details on measurements of various parameters will be provided in the following sections.

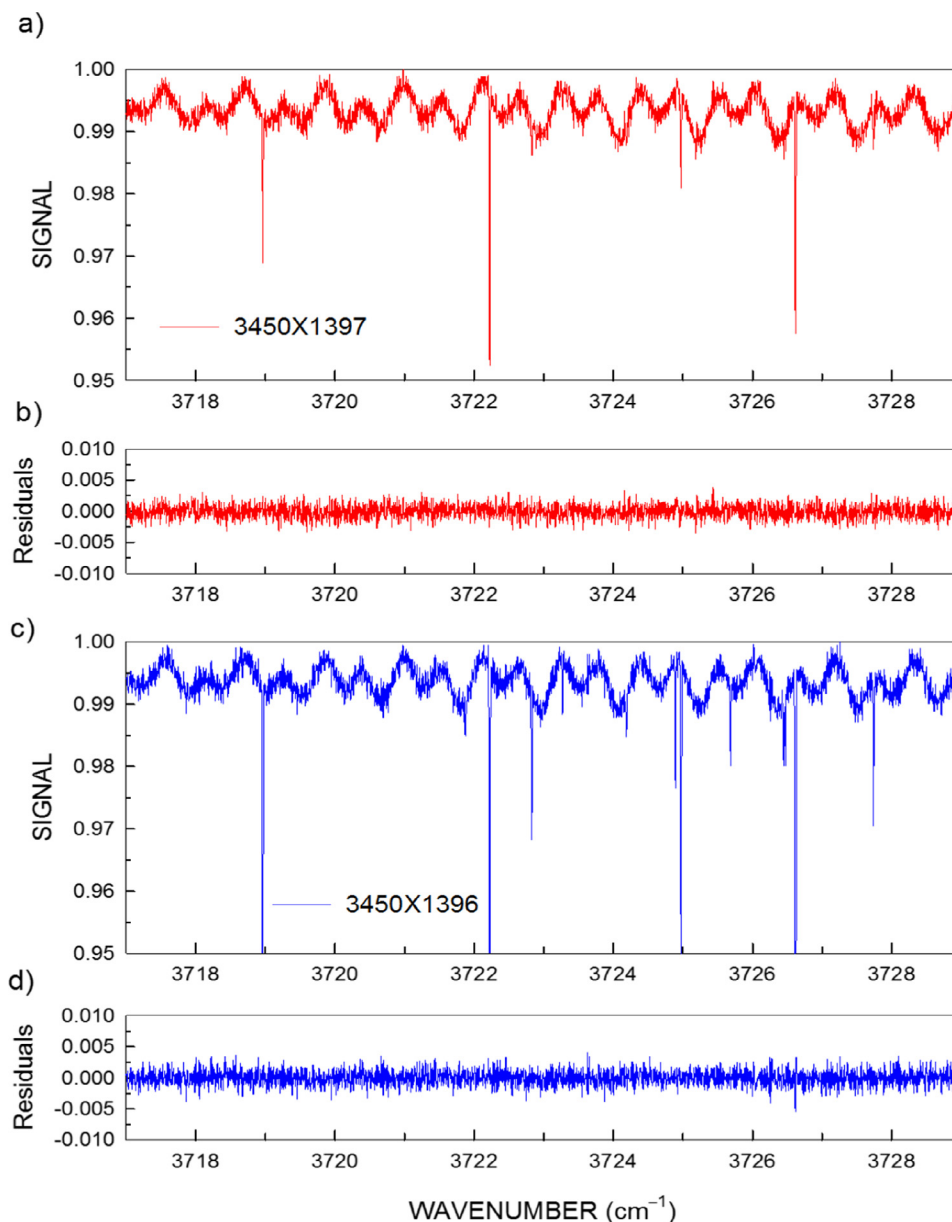


Fig. 2. Examples of channel spectra observed in two low-pressure pure water vapor spectra. 2–3 channel spectra (depending upon absorption path lengths) were observed and fitted in each spectrum by proper choice of each channel spectrum's amplitude, period and phase. Panels (a) and (c) show the two experimental low pressure pure H₂O spectra (see Table 1) while panels (b) and (d) display the corresponding weighted observed minus calculated fit residuals after considering the channel spectra in the least squares analysis. Further details are given in the text. Only the top 5% of the spectra are shown here to illustrate some details of the channel spectra.

3.3. Positions and intensities

We have compared the line positions and intensities from the present measurements with an earlier but extensive set of results by Zou and Varanasi [15] and with the recent results of Ptashnik et al. [26] and Loos et al. [27,28]. Among all of the measurements thus far published, those by Zou and Varanasi and by Loos et al. are the most extensive, providing results for a larger spectral range than the present study. Details of these comparisons will be provided in Section 6 of this paper.

3.4. Line shape parameters and their temperature dependences

Fitting the experimental spectra (Table 1) simultaneously by applying multispectrum analysis software [40,41], we were able to retrieve an accurate and self-consistent set of line parameters

especially for the air- and self-broadened half-widths and pressure-shift coefficients for the strong water vapor transitions in the 3645–3980 cm⁻¹ region. We measured the temperature dependence exponents for air-broadening and temperature dependence coefficients for air-induced pressure-shifts for the strong transitions in the ν_3 band and for a smaller number of transitions in the ν_1 band. The relationships of these parameters are given in Eqs. (1)–(3) below.

$$b_L = p \times \left[b_{L,air}^0 \times (1 - \chi) \left(\frac{T_0}{T} \right)^{n_1} + b_{L,self}^0 \times \chi \left(\frac{T_0}{T} \right)^{n_2} \right] \quad (1)$$

$$v = v_0 + p \times \left[\delta_{air}^0 \times (1 - \chi) + \delta_{self}^0 \times \chi \right] \quad (2)$$

$$\delta = \delta^0 + \delta' \times (T - T_0) \quad (3)$$

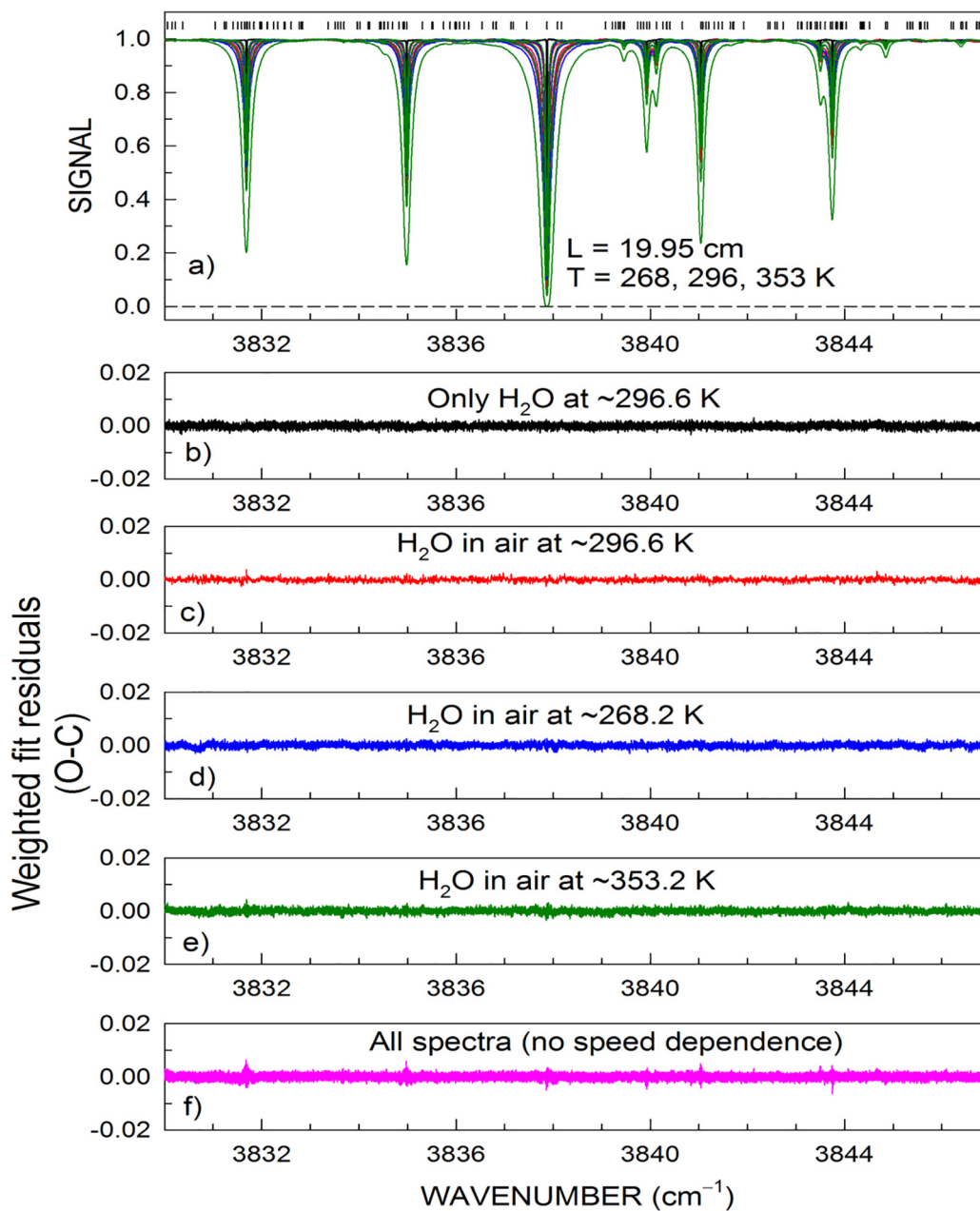


Fig. 3. A sample multispectrum fit of seven pure and 11 air-broadened water vapor spectra between 3830 and 3847 cm^{-1} . All 18 experimental spectra fitted simultaneously are plotted in panel (a) and the weighted (observed minus calculated) fit residuals in panels (b)–(e) of selected groups of spectra in different temperature ranges. Fit residuals shown in panels (b)–(e) are from the multispectrum fit of all 18 spectra. The color of each group of residuals corresponds to the color of the corresponding spectra shown in (a). The solid horizontal line at the bottom of absorption features in (a) is the 100% absorption level. The short black vertical lines above the absorption lines correspond to positions of all lines included in the fitted intervals. Details of individual spectrum conditions are given in Table 1. The last panel (f) shows the fit residuals of all 18 spectra without speed dependence included in the solution. (For interpretation of the reference to color in this figure legend, the reader is referred to the electronic version of this article).

The quantities b_L^0 and δ^0 appearing in Eqs. (1)–(3) represent the pressure broadening and pressure-shift coefficients (in $\text{cm}^{-1} \text{atm}^{-1}$ at 296 K), respectively. The parameter b_L is the Lorentz half-width (in cm^{-1}) of the spectral line at pressure p and temperature T , $b_{L,air}^0$ and $b_{L,self}^0$ are the Lorentz half-width coefficient for H_2O -air and H_2O - H_2O broadening, respectively, at the reference pressure p_0 (1 atm) and temperature T_0 (296 K) of the broadening gas, either air or H_2O in the present work, and χ is the ratio of the partial pressure of H_2O to the total sample pressure H_2O + air. Temperature dependence exponents of H_2O -air half-width coefficients (n_1) and

temperature dependence coefficients, δ'_{air} , of air-shifts were measured for a number of transitions listed in Table 2. No temperature dependences were determined for self-broadened half-width or self-shift coefficients. The linear expression given by Eq. (3) was used to model the temperature dependences of pressure-shift coefficients.

Even though line parameters were measured for over 300 individual transitions (Table 2) in the 3645–3980 cm^{-1} region, it was not possible to measure all nine line parameters (position, intensity, air-width and air-shift coefficients and their temperature dependences, self-width and self-shift coefficients at 296 K and,

Table 2
Measured line parameters and number of measurements for various line parameters obtained in the 3654–3976 cm⁻¹ region.

Parameters	Number of measurements	Parameters	Number of measurements
Position (ν) ^a	313	Intensity (S) ^b	315
Air-broadened H ₂ O half-width coefficient (H ₂ O-air width) ^c	229	Self-broadened (H ₂ O–H ₂ O) half-width coefficient (self-width) ^c	209
Temperature dependence of air-broadened H ₂ O half-width coefficient ^d (n_1)	136	(H ₂ O–H ₂ O) pressure-shift coefficient ^c (δ_{self}^0)	106
H ₂ O–air pressure-shift coefficient ^c (δ_{air}^0)	213	Off-diagonal relaxation matrix element coefficients for H ₂ O–air and H ₂ O–H ₂ O collisions ^c	10,7 ^f
Temperature dependence of H ₂ O–air pressure-shift coefficient ^e (δ_{air}^0)	128	Speed dependence (air- and self-broadened widths) ^g	85

Notes: The number of measurements for various parameters listed in the above Table includes constrained parameter values (e.g., widths, shifts and temperature dependence exponents for individual components in collision-mixed transition pairs were constrained to have identical values).

^a Line positions in cm⁻¹.

^b Line intensity in cm/molecule at 296 K.

^c Lorentz half-width and pressure-shift coefficients, and the off-diagonal relaxation matrix element coefficients in cm⁻¹ atm⁻¹ at 296 K.

^d Temperature dependence exponents of H₂O–air broadened half-width coefficients (n_1) and speed dependence parameter (no units). Only room-temperature measurements for self-broadened half-width and self-shift coefficients were measured.

^e Temperature dependence of H₂O–air pressure-shift coefficient (δ_{air}^0) in cm⁻¹ atm⁻¹ K⁻¹.

^f 10 pairs of line-mixed transitions for (H₂O–air) and seven pairs for (H₂O–H₂O) collision systems; three (H₂O–H₂O) line mixing coefficients were fixed to 0.0. See the text for details.

^g Including constrained values. No temperature dependence of speed dependence was considered, Speed dependence parameter was assumed to be the same for both air- and self-broadening.

speed dependence) for each measured transition. As listed in Table 2, the number of transitions for which parameters other than positions and intensities could be measured was limited by the weakness of the transitions and the limited optical densities of spectra available in this study. The eighty-two transitions, for which all nine parameters were measured, are listed in Table 3 for convenient comparison with results in Refs. [15,26–28] while all transitions for which at least one parameter value was retrieved in the multispectrum fits are listed in the Supplemental file available online.

Table 3 lists the vibrational ($V' \leftarrow V''$) and rotational ($J' K'_a K'_c \leftarrow J'' K''_a K''_c$) identifications of the transitions in columns 1 and 2, respectively. It may be noted that all transitions in this Table belong to the same vibrational band identified by $5 \leftarrow 1$ in column 1, which is the ν_3 band according to HITRAN [1,2] nomenclature ($V' = 5, V'' = 1$). The following columns list the measured line positions (cm⁻¹), intensities (cm⁻¹/(molecule cm⁻²)), Lorentz broadened half-width coefficients, their temperature dependence exponents, pressure-shift coefficients and their temperature dependences and lastly the speed dependence of the pressure-broadened half-width coefficients. Percent uncertainties in measured line intensities, half-width coefficients, their temperature dependence exponents and speed dependence parameters are listed in the columns next to their measured values; while measured uncertainties for positions, pressure-shift coefficients and their temperature dependences are given in parentheses next to their measured values. Line intensities, pressure-broadened half-width and pressure-shift coefficients, and speed dependence correspond to T = 296 K. The uncertainties reported in the various columns correspond to 1-sigma internal statistical errors obtained from the least squares fits. The two-row format used for the line shape parameters for each transition provides air-broadening parameters in the top row of each cell and self-broadening parameters in the bottom row. As noted in Table 3, only room-temperature values for self-width and self-shift coefficients are measured. The speed dependence parameter and its percent uncertainty listed under the last two columns show that only a single value common for both air- and self-broadened half-width coefficient has been retrieved from the present analysis. It was noted earlier that for all transitions (measured and unmeasured) default values of 0.65 and 0.0 cm⁻¹ atm⁻¹ K⁻¹ were applied for the temperature dependences of self-width coefficients (n_2) and of self-shift coefficients (δ_{self}^0), respectively.

3.5. Off-diagonal relaxation matrix element coefficients

In order to fit all spectra to their noise levels, it was necessary to include collisional line mixing for certain transition pairs, as observed from the fit residuals. In the present study we applied the formalism of Levy et al. [42] using the off-diagonal relaxation matrix element coefficients to include line mixing. Prior to this study, collisional line mixing in pressure-broadened water vapor transitions was first reported by Brown et al. [19] who measured room temperature line mixing for two pairs of H₂O transitions, one pair each in the P and R branch, for self-broadening and six other perturbers (foreign-broadening gases) (H₂, He, CO₂, air, N₂ and O₂) in the ν_2 band. Recently, line mixing via off-diagonal relaxation matrix element coefficients were reported for several transition pairs in the ν_2 , ν_1 , and the ν_3 bands of HDO broadened by CO₂ [44–46], and Rosenkranz line mixing parameters [47] were reported for air- and self-broadened H₂O transitions in the 1850–4000 cm⁻¹ region [27,28], including temperature-dependence of the Rosenkranz line mixing for six air-broadened transitions [27] over the range 250–300 K. Details of the equations used for retrieving the off-diagonal relaxation matrix element coefficients are given in Refs. [19,48] and therefore will not be repeated here. Because the air-broadened spectra analyzed in this study were recorded at different temperatures (T = 268, 296 and 353 K), variation of the relaxation matrix element coefficients with temperature was examined. No theoretical calculations of off-diagonal relaxation matrix element coefficients and their temperature dependences have been reported thus far for any water vapor transitions. However, a number of theoretical studies on pressure-broadened half-widths and line-shift coefficients for different water isotopologues involving various broadening gases have been published [29–35], including a few studies involving the temperature dependences of half-width and line-shift coefficients for the rotational transitions [35]. In the absence of any theoretical studies published on the temperature dependence of line mixing parameters (off-diagonal relaxation matrix elements) for any water vapor transitions, we have assumed the same power law expression, given by Eq. (1), used for the half-width coefficients, to be applicable for the temperature dependence of line mixing coefficients as well. However, we were unable to determine any reliable values for the temperature dependence exponents for the measured H₂O–air or H₂O–H₂O collisional line mixing coefficients. We have therefore fixed the temperature dependence

Table 3
Measured line positions, intensities and, air- and self-broadened line shape parameters for the strongest transitions in the ν_3 band of H_2^{16}O .

Vibrational quanta	Rotational quantum numbers ^a	Position and unc. ^b	Line intensity ^c	% unc.	Width (b_L^0) ^d	% unc.	T. dep. (n) ^e	% unc.	Shift (δ^0) ^d and unc.	T. dep. (δ') ^f and unc.	Speed dependence ^g	% unc.
5 ← 1	3 3 1 ← 4 3 2	3647.552909(5)	3.9068e–20	0.02	0.07986 0.45275	0.06 0.21	0.6498	0.35	–0.003072(24) +0.03200(150)	+0.041(5)	0.0932	2.3
5 ← 1	4 0 4 ← 5 0 5	3649.283053(3)	1.4542e–19	0.01	0.08778 0.54310	0.02 0.22	0.6799	0.22	–0.008648(16) –0.03052(125)	+0.239(4)	0.0948	1.2
5 ← 1	4 1 4 ← 5 1 5	3650.636109(5)	4.6465e–20	0.02	0.08425 0.53162	0.06 0.17	0.6690	0.31	–0.008273(25) –0.03570(148)	+0.259(5)	0.0889	1.9
5 ← 1	3 1 2 ← 4 1 3	3651.365171(5)	4.8515e–20	0.02	0.09201 0.52116	0.05 0.17	0.7617	0.28	–0.003646(27) –0.01935(148)	+0.082(6)	0.0817	2.1
5 ← 1	3 2 2 ← 4 2 3	3656.303543(4)	1.0066e–19	0.01	0.08863 0.51153	0.03 0.11	0.6829	0.23	–0.003227(17) +0.02370(127)	+0.007(4)	0.0971	1.3
5 ← 1	3 0 3 ← 4 0 4	3668.776579(5)	6.3754e–20	0.02	0.09463 0.55405	0.05 0.21	0.7613	0.26	–0.008368(21) +0.01069(146)	+0.205(5)	0.0888	2.0
5 ← 1	3 1 3 ← 4 1 4	3670.749725(3)	1.8199e–19	0.01	0.09188 0.52044	0.02 0.14	0.7391	0.22	–0.006296(15) +0.00318(132)	+0.152(4)	0.1138	0.9
5 ← 1	2 2 0 ← 3 2 1	3674.957865(4)	8.7249e–20	0.02	0.09319 0.50407	0.04 0.19	0.7255	0.26	–0.003961(21) –0.00679(146)	+0.008(5)	0.1139	1.0
5 ← 1	2 1 1 ← 3 1 2	3676.019555(3)	1.6951e–19	0.01	0.09712 0.47565	0.03 0.14	0.7448	0.21	–0.001715(17) –0.02265(136)	+0.027(4)	0.1418	0.5
5 ← 1	2 2 1 ← 3 2 2	3679.436265(7)	2.9231e–20	0.03	0.09212 0.51508	0.09 0.36	0.7378	0.41	–0.002977(34) –0.02261(192)	+0.013(8)	0.0940	2.9
5 ← 1	2 0 2 ← 3 0 3	3688.451403(3)	2.1638e–19	0.01	0.10028 0.52353	0.02 0.09	0.7975	0.18	–0.007969(18) –0.03552(144)	+0.271(4)	0.1304	0.7
5 ← 1	2 1 2 ← 3 1 3	3691.298176(5)	6.3327e–20	0.02	0.09666 0.53819	0.05 0.17	0.7971	0.24	–0.005427(22) –0.00706(152)	+0.154(5)	0.1138	1.4
5 ← 1	1 1 0 ← 2 1 1	3701.805704(5)	4.5122e–20	0.03	0.10310 0.48452	0.09 0.23	0.7575	0.41	–0.001666(43) –0.00932(164)	+0.024(9)	0.1341	1.6
5 ← 1	1 0 1 ← 2 0 2	3709.402295(4)	6.5867e–20	0.02	0.10408 0.47272	0.05 0.16	0.8000	0.23	–0.008845(24) –0.01230(142)	+0.262(5)	0.1122	1.4
5 ← 1	1 1 1 ← 2 1 2	3712.204495(3)	1.4215e–19	0.02	0.10122 0.57025	0.03 0.10	0.8132	0.18	–0.003487(19) –0.00484(131)	+0.108(4)	0.1175	0.9
5 ← 1	3 1 3 ← 3 1 2	3722.222317(6)	3.7466e–20	0.04	0.10125 0.53106	0.07 0.22	0.8222	0.29	–0.003760(36) +0.01528(173)	+0.062(8)	0.1033	2.0
5 ← 1	6 5 2 ← 6 5 1	3724.893608(12)	3.8903e–21	0.11	0.05395 0.25449	0.24 1.23	0.5622	2.42	–0.006256(122) +0.01173(196)	+0.243(23)	0.1137	0.0
5 ← 1	5 5 1 ← 5 5 0	3726.617094(5)	3.0717e–20	0.04	0.05146 0.27120	0.06 0.79	0.6363	0.39	–0.006422(16) –0.00311(115)	+0.201(4)	0.1163	1.1
5 ← 1	5 5 0 ← 5 5 1	3726.625450(16)	8.1400e–21	0.04	0.05146 ^h 0.27120 ^h	0.06 0.79	0.6363 ^h	0.39	–0.006422(16) ^h –0.00311(115) ^h	+0.201(4) ^h	0.1163 ^h	1.1
5 ← 1	0 0 0 ← 1 0 1	3732.134215(3)	1.2119e–19	0.02	0.10356 0.48528	0.03 0.10	0.7609	0.20	–0.002449(19) +0.00813(118)	–0.044(4)	0.1139	1.0
5 ← 1	4 2 3 ← 4 2 2	3734.272763(9)	1.5319e–20	0.04	0.09252 0.49273	0.12 0.39	0.7816	0.55	–0.004549(61) +0.00905(258)	+0.053(12)	0.0717	5.8
5 ← 1	6 4 2 ← 6 4 3	3734.644881(8)	1.3528e–20	0.04	0.07098 0.38267	0.13 0.47	0.6565	0.72	–0.002608(53) +0.00780(223)	+0.021(11)	0.1059	3.2
5 ← 1	5 4 2 ← 5 4 1	3734.930719(4)	3.5339e–20	0.02	0.06713 0.35805	0.06 0.21	0.6146	0.33	–0.005943(20) +0.00733(97)	+0.179(4)	0.1140	1.1
5 ← 1	5 4 1 ← 5 4 2	3735.444698(8)	1.1737e–20	0.06	0.06713 ^h 0.35805 ^h	0.06 0.21	0.6146 ^h	0.33	–0.005943(20) ^h +0.00733(97) ^h	+0.179(4) ^h	0.1140 ^h	1.1
5 ← 1	5 3 3 ← 5 3 2	3735.492633(4)	2.1855e–20	0.04	0.08273 0.45219	0.10 0.33	0.7496	0.51	–0.007233(50) –0.02066(197)	+0.225(10)	0.0853	3.8
5 ← 1	6 4 1 ← 4 4 0	3736.682610(4)	2.7242e–20	0.04	0.06436	0.03	0.6750	0.28	–0.005258(16)	+0.117(3)	0.1004	1.2

(continued on next page)

Table 3 (continued)

Vibrational quanta	Rotational quantum numbers ^a	Position and unc. ^b	Line intensity ^c	% unc.	Width (b_L^0) ^d	% unc.	T. dep. (n) ^e	% unc.	Shift (δ^0) ^d and unc.	T. dep. (δ') ^f and unc.	Speed dependence ^g	% unc.
5 ← 1	4 4 0 ← 4 4 1	3736.743180(3)	8.1827e–20	0.03	0.33494 0.06436 ^h 0.33494 ^h	0.14 0.03 0.14	0.6750	0.28	+0.00427(97) –0.005258(16) ^h +0.00427(97) ^h	+0.117(3) ^h	0.1004 ^h	1.2
5 ← 1	2 1 2 ← 2 1 1	3738.400727(7)	2.3979e–20	0.03	0.10173 0.52339	0.10 0.29	0.7905	0.38	–0.004931(44) +0.03742(204)	+0.045(10)	0.1045	2.7
5 ← 1	4 3 2 ← 4 3 1	3741.306224(7)	2.0324e–20	0.03	0.08138 0.40428	0.10 0.37	0.7156	0.46	–0.006339(40) –0.01145(193)	+0.223(9)	0.1153	2.3
5 ← 1	4 3 1 ← 4 3 2	3743.946449(5)	5.6577e–20	0.03	0.08090 0.42272	0.06 0.19	0.7061	0.31	–0.00266(22) +0.02788(138)	+0.087(5)	0.1023	1.8
5 ← 1	3 2 2 ← 3 2 1	3744.509479(4)	1.0312e–19	0.03	0.09475 0.49111	0.06 0.13	0.7350	0.30	–0.005570(34) +0.02622(152)	+0.054(5)	0.1257	1.2
5 ← 1	3 3 1 ← 3 3 0	3744.651240(3)	1.6470e–19	0.04	0.07779 0.39568	0.05 0.11	0.6947	0.32	–0.005122(25) +0.01098(136)	+0.123(4)	0.1001	1.4
5 ← 1	3 3 0 ← 3 3 1	3745.086704(5)	5.4846e–20	0.03	0.07805 0.39294	0.06 0.20	0.6951	0.32	–0.003487(21) +0.01731(138)	+0.079(5)	0.0987	2.0
5 ← 1	1 1 1 ← 1 1 0	3749.329153(3)	1.6139e–19	0.03	0.10300 0.48272	0.04 0.10	0.7293	0.22	–0.007617(18) +0.01396(128)	+0.187(4)	0.1077	1.2
5 ← 1	2 2 1 ← 2 2 0	3749.573789(4)	7.3092e–20	0.03	0.09188 0.50058	0.05 0.15	0.7274	0.29	–0.004615(22) –0.005102(141)	+0.038(5)	0.1004	1.9
5 ← 1	2 2 0 ← 2 2 1	3752.212617(3)	2.1784e–19	0.03	0.09207 0.49482	0.03 0.09	0.7123	0.22	0.003649(17) –0.06115(125)	+0.103(4)	0.1186	1.0
5 ← 1	3 2 1 ← 3 2 2	3756.616451(6)	3.3386e–20	0.03	0.09238 0.48502	0.06 0.26	0.7208	0.35	–0.002451(32) –0.06420(174)	+0.123(7)	0.0705	3.7
5 ← 1	1 1 0 ← 1 1 1	3759.844496(5)	5.3490e–20	0.03	0.10269 0.51971	0.05 0.18	0.7339	0.27	+0.001493(27) –0.02833(154)	–0.026(6)	0.0938	1.9
5 ← 1	4 2 2 ← 4 2 3	3765.760277(5)	4.4535e–20	0.03	0.09386 0.52170	0.05 0.20	0.7320	0.30	–0.002623(28) –0.03272(157)	+0.098(6)	0.1016	1.8
5 ← 1	2 1 1 ← 2 1 2	3769.888988(5)	7.1630e–20	0.03	0.10181 0.54520	0.05 0.15	0.7421	0.24	–0.0010439(24) –0.03661(147)	+0.039(5)	0.1050	1.5
5 ← 1	1 0 1 ← 0 0 0	3779.493135(7)	4.2344e–20	0.03	0.10396 0.48063	0.07 0.27	0.7778	0.28	–0.005051(37) –0.00530(208)	+0.202(8)	0.1081	1.9
5 ← 1	5 2 3 ← 5 2 4	3779.762272(19)	6.3317e–21	0.11	0.09269 0.50954	0.28 0.80	0.7799	1.26	–0.004260(142) –0.03944(519)	+0.194(29)	0.1206	5.9
5 ← 1	3 1 2 ← 3 1 3	3784.583804(12)	1.2400e–20	0.05	0.09944 0.52665	0.14 0.48	0.7683	0.69	–0.002995(60) –0.03098(323)	+0.100(F)	0.0780	6.6
5 ← 1	2 1 2 ← 1 1 1	3796.439552(5)	5.1640e–20	0.02	0.10079 0.57438	0.06 0.17	0.7963	0.25	–0.002924(25) –0.01152(155)	+0.044(6)	0.1124	1.5
5 ← 1	2 0 2 ← 1 0 1	3801.418689(3)	2.169e–19	0.01	0.10244 0.45943	0.02 0.08	0.7800	0.17	+0.001839(17) +0.01591(130)	–0.110(4)	0.1290	0.7
5 ← 1	2 1 1 ← 1 1 0	3807.013666(3)	1.4881e–19	0.01	0.10196 0.47217	0.03 0.10	0.7566	0.19	–0.005061(17) +0.00423(128)	+0.113(4)	0.1332	0.7
5 ← 1	3 1 3 ← 2 1 2	3816.091708(3)	2.1334e–19	0.04	0.09660 0.53275	0.03 0.09	0.8228	0.17	–0.002809(16) +0.00213(126)	+0.077(4)	0.1094	0.9
5 ← 1	3 0 3 ← 2 0 2	3820.738533(4)	8.1246e–20	0.03	0.09906 0.52530	0.04 0.13	0.8209	0.19	+0.006586(21) +0.03247(131)	–0.118(4)	0.1206	0.9
5 ← 1	3 2 2 ← 2 2 1	3821.764198(4)	9.6616e–20	0.03	0.09244 0.53609	0.03 0.12	0.7768	0.21	–0.004816(18) +0.00487(126)	+0.178(4)	0.1016	1.0
5 ← 1	3 2 1 ← 2 2 0	3826.753905(6)	3.2301e–20	0.03	0.09265 0.51427	0.06 0.25	0.7940	0.31	–0.002937(31) +0.00294(172)	+0.149(7)	0.0983	2.2
5 ← 1	3 1 2 ← 2 1 1	3831.686304(3)	6.4733e–20	0.02	0.09808 0.47214	0.05 0.15	0.7903	0.23	–0.007410(21) –0.00028(134)	+0.212(4)	0.1426	0.9
5 ← 1	4 1 4 ← 3 1 3	3834.983083(4)	6.9062e–20	0.02	0.09085 0.51778	0.04 0.14	0.7815	0.23	–0.003089(19) –0.01483(127)	+0.087(4)	0.1014	1.4

Table 3 (continued)

Vibrational quanta	Rotational quantum numbers ^a	Position and unc. ^b	Line intensity ^c	% unc.	Width (b_l^0) ^d	% unc.	T. dep. (n) ^e	% unc.	Shift (δ^0) ^d and unc.	T. dep. (δ') ^f and unc.	Speed dependence ^g	% unc.
5 ← 1	4 0 4 ← 3 0 3	3837.869274(3)	2.2627e–19	0.02	0.09449 0.55835	0.02 0.08	0.8051	0.17	+0.002226(16) –0.00332(121)	–0.030(4)	0.1123	0.9
5 ← 1	4 3 1 ← 3 3 0	3841.044816(5)	4.3007e–20	0.02	0.08056 0.45808	0.05 0.21	0.7525	0.29	–0.005008(23) –0.005428(138)	+0.106(5)	0.0949	1.9
5 ← 1	4 2 3 ← 3 2 2	3843.750878(5)	3.8461e–20	0.02	0.08774 0.48491	0.06 0.22	0.7490	0.31	–0.006599(27) –0.04377(151)	+0.250(6)	0.0808	2.7
5 ← 1	5 1 5 ← 4 1 4	3852.057460(3)	1.799e–19	0.02	0.08285 0.50371	0.02 0.10	0.6641	0.21	–0.002941(14) +0.03225(113)	+0.048(3)	0.1025	0.9
5 ← 1	4 2 2 ← 3 2 1	3853.966209(4)	1.1795e–19	0.02	0.09060 0.45531	0.06 0.13	0.7259	0.25	–0.004828(27) –0.01779(136)	+0.113(4)	0.1093	1.2
5 ← 1	4 1 3 ← 3 1 2	3854.438182(3)	1.7698e–19	0.02	0.09371 0.48978	0.03 0.10	0.7600	0.20	–0.006200(18) +0.00503(125)	+0.180(3)	0.1132	0.8
5 ← 1	5 3 3 ← 4 3 2	3861.787793(5)	4.3852e–20	0.02	0.07651 0.41061	0.05 0.22	0.6398	0.33	–0.006813(21) –0.01382(130)	+0.224(5)	0.0903	2.0
5 ← 1	5 2 4 ← 4 2 3	3865.111525(4)	8.7287e–20	0.01	0.08366 0.48558	0.04 0.14	0.6489	0.25	–0.005867(16) –0.00470(115)	+0.176(4)	0.0804	1.8
5 ← 1	6 1 6 ← 5 1 5	3869.192640(5)	4.3259e–20	0.02	0.07212 0.44219	0.06 0.27	0.5633	0.40	–0.003755(20) –0.03725(139)	+0.138(5)	0.0989	1.8
5 ← 1	6 0 6 ← 5 0 5	3870.129400(3)	1.3071e–19	0.02	0.07502 0.46601	0.03 0.14	0.5687	0.28	–0.002437(14) –0.02159(118)	+0.066(3)	0.1122	1.0
5 ← 1	5 1 4 ← 4 1 3	3874.402204(5)	4.3610e–20	0.02	0.08965 0.48423	0.06 0.26	0.7571	0.29	–0.003841(25) +0.02435(149)	+0.048(6)	0.1067	1.7
5 ← 1	5 2 3 ← 4 2 2	3880.191418(6)	3.2252e–20	0.04	0.09002 0.42255	0.09 0.35	0.7992	0.34	–0.008579(37) –0.04145(172)	+0.274(7)	0.0841	1.5
5 ← 1	6 2 5 ← 5 2 4	3880.354707(8)	2.0277e–20	0.04	0.07755 0.44962	0.10 0.43	0.6602	0.56	–0.006581(41) –0.02845(209)	+0.220(9)	0.0831	4.0
5 ← 1	7 1 7 ← 6 1 6	3885.659922(4)	8.2167e–20	0.02	0.06053 0.41281	0.03 0.25	0.4314	0.49	–0.005205(16) +0.00543(152)	+0.245(3)	0.1244	1.0
5 ← 1	7 0 7 ← 6 0 6	3886.077259(6)	2.7546e–20	0.03	0.06122 0.40657	0.08 0.38	0.4374	0.66	–0.004804(23) –0.00560(156)	+0.188(5)	0.1118	1.9
5 ← 1	6 1 5 ← 5 1 4	3891.299500(4)	8.2439e–20	0.02	0.08422 0.48291	0.04 0.21	0.7240	0.26	–0.001818(18) +0.01712(130)	+0.080(4)	0.0825	1.8
5 ← 1	7 2 6 ← 6 2 5	3899.441416(5)	4.3166e–20	0.02	0.06846 0.39714	0.06 0.33	0.5620	0.46	–0.007623(20) –0.02657(140)	+0.309(5)	0.1016	1.8
5 ← 1	8 1 8 ← 7 1 7	3901.666439(7)	1.5536e–20	0.04	0.04872 0.33904	0.12 0.63	0.3387	1.36	–0.007656(29) –0.00579(203)	+0.323(6)	0.1238	2.4
5 ← 1	8 0 8 ← 7 0 7	3701.846942(4)	4.7063e–20	0.02	0.04916 0.35210	0.06 0.34	0.3487	0.80	–0.006893(14) +0.00249(125)	+0.300(3)	0.1414	1.0
5 ← 1	6 2 4 ← 5 2 3	3904.188663(5)	6.2507e–20	0.02	0.08980 0.44701	0.04 0.26	0.8442	0.26	–0.010112(24) –0.01733(143)	+0.282(5)	0.0686	2.4
5 ← 1	7 3 5 ← 6 3 4	3904.294965(8)	2.0004e–20	0.04	0.07091 0.38176	0.08 0.54	0.6833	0.64	–0.010097(44) –0.05943(210)	+0.336(9)	0.0686	2.4
5 ← 1	8 2 7 ← 7 2 6	3916.328740(12)	7.6223e–21	0.07	0.05850 0.34959	0.19 0.78	0.4763	1.53	–0.007960(69) +0.02588(327)	+0.304(14)	0.1180	3.7
5 ← 1	9 1 9 ← 8 1 8	3917.285843(6)	2.3916e–20	0.05	0.03845 0.31084	0.10 0.47	0.2782	1.40	–0.009660(20) –0.00976(161)	+0.382(4)	0.1449	1.3
5 ← 1	9 0 9 ← 8 0 8	3917.362738(10)	8.0222e–21	0.08	0.03832 0.32391	0.21 0.79	0.2462	2.96	–0.009508(41) –0.02155(270)	+0.386(9)	0.1589	2.3
5 ← 1	8 1 7 ← 7 1 6	3920.088775(7)	2.3845e–20	0.04	0.06613 0.41709	0.08 0.38	0.5513	0.62	–0.002285(33) +0.01892(185)	–0.014(7)	0.1174	1.7
5 ← 1	7 3 4 ← 6 3 3	3925.134338(16)	6.7952e–21	0.11	0.09275 0.47332	0.44 0.71	0.8176	1.30	–0.01874(30) –0.03337(210)	+0.670(34)	0.1517	1.3
5 ← 1	7 2 5 ← 6 2 4	3925.175901(11)	1.0943e–20	0.09	0.09405	0.32	0.8745	0.77	–0.007859(27)	+0.304(22)	0.1517 ^h	1.3

(continued on next page)

Table 3 (continued)

Vibrational quanta	Rotational quantum numbers ^a	Position and unc. ^b	Line intensity ^c	% unc.	Width (b_1^d) ^d	% unc.	T. dep. (n) ^e	% unc.	Shift (δ^f) ^d and unc.	T. dep. (δ^f) ^f and unc.	Speed dependence ^g	% unc.
5 ← 1	8 2 6 ← 7 2 5	3942.652393(9)	1.5313e–20	0.05	0.48481 0.08167	0.52 0.12	0.8376	0.59	–0.03337(210) ^h –0.008492(67)	+0.314(13)	0.0984	3.1
5 ← 1	9 3 7 ← 8 3 6	3942.887054(15)	5.2038e–21	0.08	0.47480 0.06023	0.48 0.27	0.5601	1.92	+0.03883(254) –0.01232(106)	+0.427(21)	0.1507	3.1
5 ← 1	10 1 9 ← 9 1 8	3948.177129(9)	4.5535e–21	0.06	0.36116 0.04092	1.02 0.24	0.2874	3.9	–0.01910(393) –0.006899(74)	+0.273(13)	0.1689	2.2
5 ← 1	8 3 5 ← 7 3 4	3949.983713(12)	1.0530e–20	0.05	0.31593 0.08896	0.98 0.16	0.9354	0.69	–0.005(F) –0.012090(98)	+0.491(19)	0.1167	3.1
					0.47575	0.57			–0.03868(317)			

The uncertainties listed under the various columns correspond to one sigma internal statistical uncertainty obtained from the least-squares fits. In the two row format, the numbers in the top row in each cell correspond to air-broadening of H₂O, and the bottom numbers correspond to self-broadening of H₂O.

^a For all transitions, the temperature dependences of self-broadened half-width coefficients (b_2) and self-shift coefficients (δ') were fixed to 0.75 and 0.0, respectively.

^b For the first column, HITRAN [1,2] vibrational codes $V \leftarrow V''$; for the second column $J' K_a' K_c' \leftarrow J'' K_a'' K_c''$.

^c Positions and uncertainties in cm^{–1}.

^d Line intensities (S) in cm/molecule at 296 K.

^e Lorentz half-width coefficients (b_1^d) and pressure-shift coefficients (δ^f) in cm^{–1} atm^{–1} at 296 K. Pressure-shift uncertainties are given in parentheses in units of the last digit quoted.

^f The temperature dependence exponents of broadening coefficients or self-broadening or self-shift coefficients were measured.

^g Temperature dependences of pressure shift coefficients, δ' (H₂O-air) in units of 10^{–4} cm^{–1} atm^{–1} K^{–1}. Uncertainties are given in parentheses in units of the last digit quoted.

^h Speed dependence parameter has no units. The speed dependence parameters for both air- and self-broadening are assumed to be the same and hence only one value for each transition is determined.

ⁱ Value were constrained to be identical to that of the transition listed just above it in this table; for example see 5 5 1 ← 5 5 0 and 5 5 0 ← 5 5 1 (see the text for further details).

exponent to a constant value of 0.7 (a value usually used as a default value for the temperature dependence exponent of unmeasured (or weak) pressure-broadened half-width coefficients). It may be recalled that in the case of methane, Tran et al. [49] computed relaxation matrix element coefficients and their temperature dependence exponents (where a power law model given by Eq. (1) was applied to model the temperature dependence of off-diagonal relaxation matrix element coefficients) for the ν_3 and ν_4 bands of ¹²CH₄ for all theoretically predicted line pairs.

An example of a multispectrum fit where collisional line mixing was observed and quantified in the ν_3 band of air-broadened H₂O is displayed in Fig. 4. To show details, a shorter segment (3851–3857 cm^{–1}) from a wider fit interval (3847–3867 cm^{–1}) of all 18 spectra is plotted in the top panel (a). The weighted residuals resulting from the multispectrum fit with a Voigt line shape profile including line mixing (off-diagonal relaxation matrix element coefficients) and quadratic speed dependence parameter are plotted in the middle panel (b). In the bottom panel (c), the residuals from the same fit without taking into account the line mixing (but including speed dependence) are shown (see Tables 1 and 4 for details). The dotted horizontal line at the bottom of (a) represents the fully absorbing level (0% transmission level) and the short vertical lines at the top of (a) correspond to positions of absorption lines included in the fitted interval. There are 230 water vapor lines included in this spectral interval. Line mixing occurring between the pairs of transitions marked 1 and 4, 3 and 5, 3 and 4, and 4 and 5 was measured; mixing parameters for H₂O-air collisions were determined for three of these sets, and mixing parameters for H₂O-H₂O collisions were determined for two sets (both mixing coefficients were not measured for all four mixed sets). As noted above, temperature dependence exponents of the collisional line mixing coefficients were fixed to a default value of 0.7 for all four pairs of lines shown in the figure.

In the present study (PS), line mixing via off-diagonal relaxation matrix element coefficients, W_{ij} (cm^{–1} atm^{–1} at 296 K), were measured for 12 pairs of transitions which included ten H₂O-air and seven H₂O-H₂O collision systems. Among the 12 transition pairs for which collisional mixing coefficients were measured there were only 5 pairs of transitions for which both H₂O-air and H₂O-H₂O mixing was measured. In all five cases, the line mixing coefficient for the H₂O-H₂O system was larger than for H₂O-air. The measured off-diagonal relaxation matrix element coefficients (ORME), W_{ij} (cm^{–1} atm^{–1} at 296 K), for the H₂O-air and H₂O-H₂O collision systems in the ν_3 band are listed in Table 4. As noted in the table, we were able to determine from the multispectrum fits only one value for the temperature-dependence exponent of the air-broadened mixing coefficient, for the pair 2 2 0 ← 3 2 1 and 2 1 1 ← 3 1 2 near 3675 cm^{–1}; all other mixed pairs had the temperature exponent of line mixing held fixed to the default value of 0.70. No line mixing was observed for any of the ν_1 , 2 ν_2 or the $\nu_2 + \nu_3 - \nu_2$ band transitions appearing in our spectra.

For some transition pairs whose line positions are close to each other (e.g., the 5 5 1 ← 5 5 0 and 5 5 0 ← 5 5 1 transitions located at 3726.6171 and 3726.6255 cm^{–1}, respectively), even though the two line positions and intensities were separately determined, their air widths, air-shifts and the temperature dependences were constrained to be identical. For such close transitions, auxiliary parameters and constraints were setup such that the line separation between the two components and their intensity ratio could either be fixed to theoretical values (if the separation is too small) or adjusted in the fits, if needed, to minimize the residuals. This flexibility will allow the line separation and intensity ratio to remain close to theoretical values so that realistic values of line shape parameters can be determined. Similarly, if the two components in a line-mixed set are well separated, such that the two positions and two intensities could be determined accurately

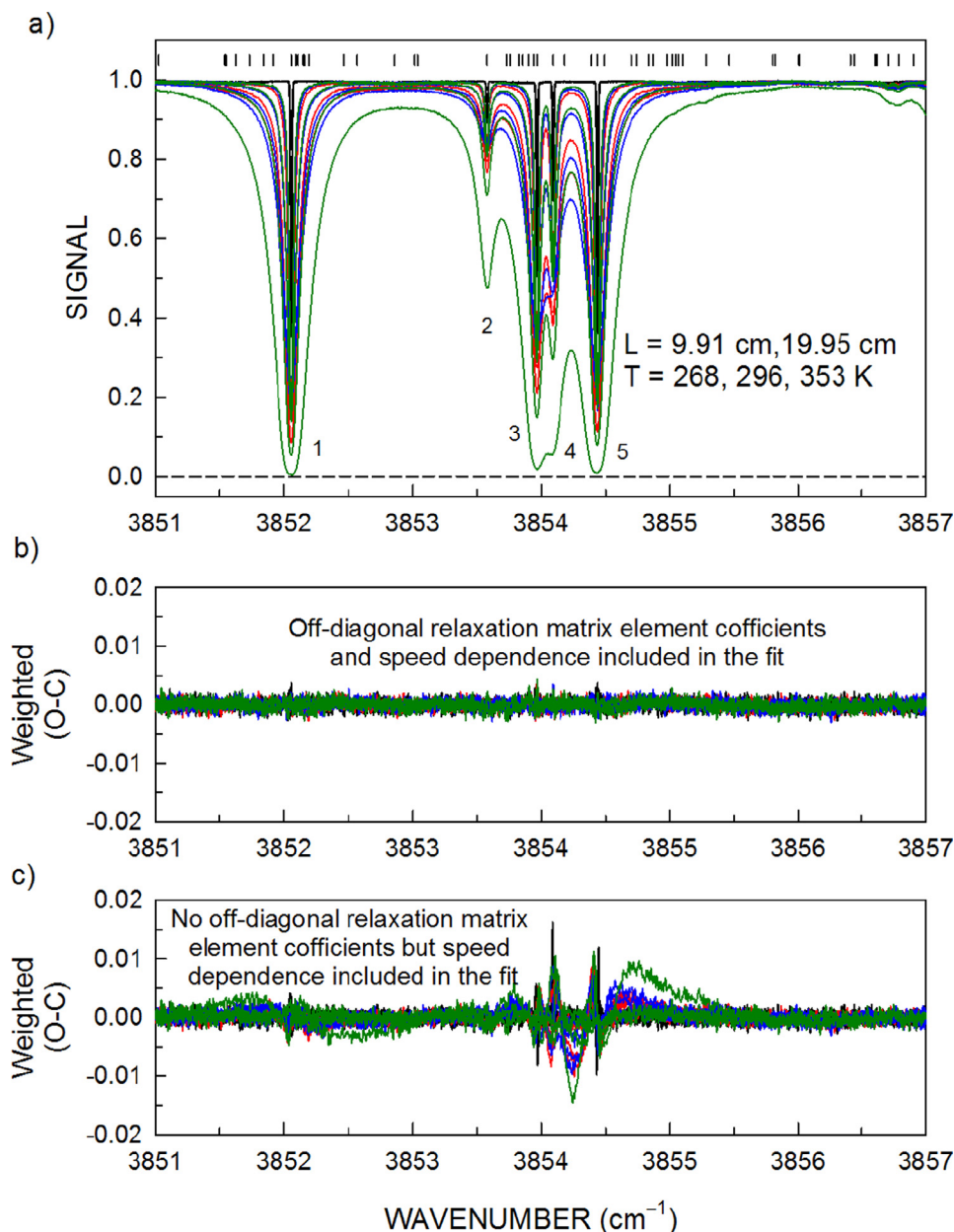


Fig. 4. A short segment (3851–3857 cm⁻¹) from a 20 cm⁻¹ wide fit (3847–3867 cm⁻¹) where all 18 spectra (Table 1) were fitted simultaneously is plotted in the top panel (a). The weighted fit residuals (observed minus calculated) resulting from the multispectrum fit with a Voigt line shape profile including line mixing using the off-diagonal relaxation matrix formalism and quadratic speed dependence parameter are plotted in (b). In the bottom panel (c) the residuals from the fit without considering line mixing (but with speed dependence) are shown. See Tables 1 and 4 for details. The dotted horizontal line at the bottom of absorption features in (a) represents the 0% transmission level and the short black vertical lines at the top of absorption lines indicate the positions of lines included in the fitted region. Line mixing is occurring between the pairs of transitions marked 1 and 4, 3 and 5, 3 and 4, and 4 and 5 (see the text for details).

(for example, the 5 4 2 ← 5 4 1 and 5 4 1 ← 5 4 2 transitions located at 3734.9307 and 3735.4447 cm⁻¹, respectively), their line shape parameters could be measured independently or still be constrained to have identical values. Parameter values retrieved using constraints are indicated by a superscript *g* in Table 4.

We note that for the 7 3 4 ← 6 3 3 and 7 2 5 ← 6 2 4 transition pair near 3925 cm⁻¹ appearing in the last row of Table 4, Rosenkranz line mixing parameters were also reported in Table 10 of Ref. [27]. A rough comparison may be made by estimating the ORME from Ref. [27] as the Rozenkranz coefficient times the spacing between the pair of mixed lines ($W_{ij} \approx Y_a \times \Delta\nu$). The off-diagonal relaxation matrix element (ORME) coefficients thus estimated

from Ref. [27] are 0.036 and 0.022 cm⁻¹ atm⁻¹, while the ORME determined in the present study is 0.017 cm⁻¹ atm⁻¹.

3.6. Speed dependence parameter

A quadratic speed dependence model [43] for the half-width coefficients was applied to describe the Lorentz width as a function of velocity. The expression used to measure the speed dependence parameter is the same as applied in several of our previous studies [44–46] and hence will not be given here. For transitions for which speed dependence was not measured, the value of the speed dependence parameter was fixed to 0.1 (see the Supplementary file).

Table 4
Off-diagonal relaxation matrix element coefficients, W_{ij} ($\text{cm}^{-1} \text{atm}^{-1}$ at 296 K), for H_2O -air and H_2O - H_2O collision systems in the ν_3 band of H_2O .

#	Quantum Assignment ^a	ν (cm^{-1})	S^b	H_2O -air Width ^c	H_2O -air n^d	$\delta^0(\text{H}_2\text{O-air})^c$	$\delta'(\text{H}_2\text{O-air})^e$	W_{ij} $\text{H}_2\text{O-air}^c$	W_{ij} $\text{H}_2\text{O-H}_2\text{O}^c$
1	3 3 0 ← 4 3 1	3646.463642	1.306e-20	0.08159(7)	0.692(5)	-0.00309(6)	+0.35(4)e-05	0.0044(1)	0.0(F)
	3 2 1 ← 4 2 2	3647.138304	3.296e-20	0.08963(4)	0.731(3)	-0.00286(3)	+0.35(4)e-05 ^g		
2	4 1 4 ← 5 1 5	3650.636109	4.647e-20	0.08425(5)	0.669(2)	-0.00827(3)	+2.59(5)e-05	0.0029(1)	0.0(F)
	3 1 2 ← 4 1 3	3651.365171	4.852e-20	0.09201(5)	0.762(2)	-0.00365(3)	+0.82(6)e-05		
3	2 2 0 ← 3 2 1	3674.957865	8.725e-20	0.09319(4)	0.726(2)	-0.00396(2)	+0.78(48)e-06	0.0078(1) ^f	0.031(5)
	2 1 1 ← 3 1 2	3676.019555	1.695e-19	0.09712(3)	0.745(2)	-0.00172(2)	+0.27(4)e-05		
4	5 5 1 ← 5 5 0	3726.617089	3.072e-20	0.05136(4)	0.636(3)	-0.00642(2)	+2.00(4)e-05	0.0(F)	0.026(4)
	5 5 0 ← 5 5 1	3726.625468	8.140e-21	0.05136(4) ^g	0.636(3) ^g	-0.00642(2) ^g	+2.00(4)e-05 ^g		
5	5 4 2 ← 5 4 1	3734.930719	3.534e-20	0.06713(4)	0.615(2)	-0.00594(2)	+1.79(4)e-05	0.0013(1)	0.121(7)
	5 4 1 ← 5 4 2	3735.444698	1.174e-20	0.06713(4) ^g	0.615(2) ^g	-0.00594(2) ^g	+1.79(4)e-05 ^g		
6	3 2 2 ← 3 2 1	3744.509479	1.031e-19	0.09475(6)	0.735(2)	-0.00557(3)	+0.54(5)e-05	0.0049(0)	0.040(1)
	3 3 1 ← 3 3 0	3744.651240	1.647e-19	0.07779(4)	0.695(2)	-0.00512(3)	+0.123(4)e-04		
7	3 0 3 ← 2 0 2	3820.738533	8.125e-20	0.09906(4)	0.821(2)	+0.00066(2)	-0.119(4)e-04	0.0025(1)	0.0(F)
	3 2 2 ← 2 2 1	3821.764198	9.662e-20	0.09244(3)	0.777(2)	-0.00482(2)	+0.178(4)e-04		
8	5 0 5 ← 4 0 4	3854.090481	6.179e-20	0.08615(4)	0.688(3)	-0.00128(4)	-0.21(6)e-05	0.0035(1)	0.048(3)
	4 1 3 ← 3 1 2	3854.438182	1.770e-19	0.09371(3)	0.760(2)	-0.00620(2)	+1.80(3)e-05		
9	5 0 5 ← 4 0 4	3854.090481	6.179e-20	0.08615(4)	0.688(3)	-0.00128(4)	-0.21(6)e-05	0.0(F)	0.033(1)
	4 2 2 ← 3 2 1	3853.966209	1.180e-19	0.09060(5)	0.726(2)	-0.00483(3)	+1.13(4)e-05		
10	4 2 2 ← 3 2 1	3853.966209	1.180e-19	0.09060(5)	0.726(2)	-0.00483(3)	+1.13(4)e-05	0.0094(1)	0.0(F)
	4 1 3 ← 3 1 2	3854.438182	1.770e-19	0.09371(3)	0.760(2)	-0.00620(2)	+1.80(3)e-05		
11	5 0 5 ← 4 0 4	3854.090481	6.179e-20	0.08615(4)	0.688(3)	-0.00128(4)	-0.21(6)e-05	0.0118(1)	0.0(F)
	5 1 5 ← 4 1 4	3852.057460	1.800e-19	0.08285(2)	0.664(1)	-0.00294(1)	+0.48(3)e-05		
12	7 3 4 ← 6 3 3	3925.134434	6.795e-21	0.09275(41)	0.818(11)	-0.01874(30)	+0.67(3)e-04	0.0170(3)	0.071(2)
	7 2 5 ← 6 2 4	3925.175901	1.094e-20	0.09405(30)	0.875(7)	-0.00786(27)	+0.30(2)e-04		

(F) appearing under the last two columns indicates those values are fixed to 0.0.

^a $J' K'_a' K'_c' \leftarrow J'' K''_a'' K''_c''$.

^b Intensities (S) in $\text{cm}/\text{molecule}$ at 296 K.

^c Lorentz half-width coefficients (b^0), pressure-shift coefficients (δ^0) and off-diagonal relaxation matrix element (ORME) coefficients (line mixing), W_{ij} , in $\text{cm}^{-1} \text{atm}^{-1}$ at 296 K. Uncertainties listed in parentheses correspond to parameter values in units of the last digits quoted.

^d Temperature dependence exponents of H_2O -air half-width coefficients have no units. Uncertainties listed in parentheses correspond to parameter values in units of the last digits quoted.

^e Temperature dependences of pressure-shift coefficients, δ' (H_2O -air) in $(\text{cm}^{-1} \text{atm}^{-1} \text{K}^{-1})$.

^f Temperature dependence exponent of line mixing (unitless) determined to be 0.69(6) for this air-broadened pair of transitions only. In all other cases the temperature dependence exponent of line mixing was fixed to 0.70.

^g Value is constrained in the least squares fit to that listed in the line just above it.

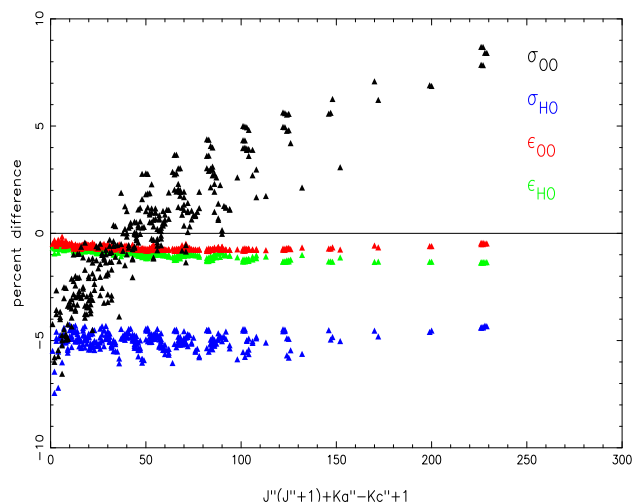


Fig. 5. The percent difference in the oxygen-broadened half-width versus an energy ordered index, $J''(J''+1)+K''_a''-K''_c''+1$, for 325 ν_2 transitions of water vapor for changes in the atom-atom parameters. Shown are the percent differences (pot 0-pot i) where $i = 1-4$ corresponding to changes in ϵ_{HO} (green points), ϵ_{00} (red points), σ_{HO} (blue points), and σ_{00} (black points). (For interpretation of the references to color in this figure legend, the reader is referred to the web version of this article.)

4. Theoretical formalism

The calculations of the line shape parameters, the half-width and line (pressure)-shift coefficients, were made using the complex formalism of Robert and Bonamy [50] as modified by Ma et al. [51] and is labeled as the Modified Complex Robert-Bonamy (MCRB) for-

mulation. The half-width, γ , and line shift, δ , of a ro-vibrational transition $f \leftarrow i$ are given by real and imaginary parts of the complex valued expression:

$$(\gamma - i\delta)_{f \leftarrow i} = \frac{n_2}{2\pi c} \times \int_0^\infty v f(v) dv \int_0^\infty 2\pi b db \left[1 - e^{-i(S_1 + \text{Im}(S_2))J_2} e^{-\text{Re}(S_2)J_2} \right] \quad (4)$$

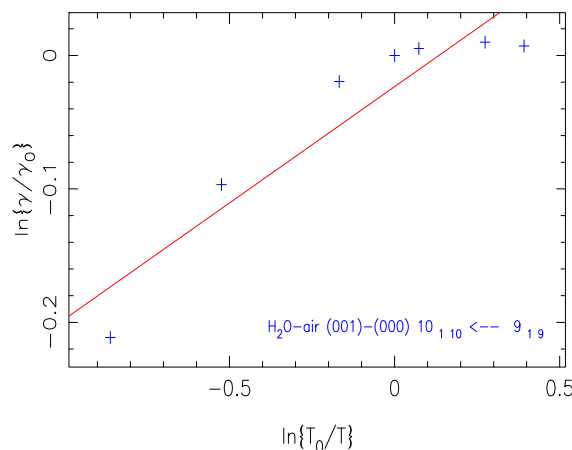


Fig. 5A. $\ln\{\gamma/\gamma_0\}$ versus $\ln\{T_0/T\}$ in the temperature range 200–700 K for the 10 10 ← 9 1 9 transition of the ν_3 band of H_2O . Blue + symbols are the data points, solid red line is the least-squares fit of the data. The slope of the line is the temperature exponent, n . (For interpretation of the references to color in this figure legend, the reader is referred to the web version of this article.)

where n_2 is the number density of perturbers, v is the velocity, $f(v)$ is the Boltzmann distribution of velocity, $\langle \rangle_{j_2}$ is the average over the states of the perturber, and b is the impact parameter. S_1 and S_2 are the first and second order terms in the successive expansion of the Liouville scattering matrix and depend on the intermolecular potential.

The intermolecular potential consists of the electrostatic components (dipole-dipole (H₂O–H₂O), dipole-quadrupole and quadrupole-quadrupole), an atom-atom component described by the Lennard-Jones potential [52,53], and the induction and London dispersion terms give the isotropic components. In order to employ the atom-atom potential in the formalism, the r_{ij} atom-atom distances must be mapped into the center of mass separation, R , using the expansion of Sack [54]. The expansion is described in terms of the Order and the Rank (ℓ_1, ℓ_2) of the Wigner D-matrices for the radiating (labeled 1) and perturbing (labeled 2) molecule. Here, the atom-atom part of the potential was expanded to 20th Order and Rank 4, 4 for the N₂- and O₂-broadening calculations and to 8th Order and Rank 2, 2 for the self-broadening calculations. The isotropic part of the atom-atom potential was used in Hamilton's equations of motion to solve for the trajectories of the collision pairs. The calculations included the real and imaginary components for the half-width and line shift coefficients and proper averaging over the velocity, both of which have been shown to be important [22,55–58].

The parameters describing the electrostatic, induction, and London dispersion potentials (dipole moments, quadrupole moments, ionization potentials, etc.) are well known. The Lennard-Jones atom-atom potential is:

$$V_{atom-atom} = \sum_{ij} 4\epsilon_{ij} \left[\left(\frac{\sigma_{ij}}{r_{ij}} \right)^{12} - \left(\frac{\sigma_{ij}}{r_{ij}} \right)^6 \right] \quad (5)$$

where the sum on i and j are over the atoms on the radiating and perturbing molecules. The parameters ϵ_{ij} and σ_{ij} are somewhat in question. There are a number of proposed methods to determine heteronuclear atom-atom parameters from homonuclear parameters [53,59–64]. Using the different combination rules lead to some differences in the derived ϵ_{ij} parameters greater than 1900% with many combinations different by several hundred percent and differences in the derived σ_{ij} parameters >35%.

The atom-atom parameters for the H₂O–N₂ collision system were adjusted previously [65]. For the H₂O–O₂ collision system, starting atom-atom parameters (pot 0) were determined using the combination rules of Hirschfelder et al. [53] with the homonuclear atom-atom parameters of Bouanich [60]. Initial calculations changing each atom-atom parameter (ϵ_{HO} , ϵ_{OO} , σ_{HO} , σ_{OO}) by 5% were made to see the effect these parameters have on the calculated half-width. Fig. 5 shows the percent difference in the oxygen-broadened half-width versus an energy ordered index for 325 ν_2 transitions of water vapor selected from the intercomparison database [31] for changes in the atom-atom parameters. Shown are the percent differences (pot 0–pot i) where $i = 1, 4$ corresponding to ϵ_{HO} (green points), ϵ_{OO} (red points), σ_{HO} (blue points), and σ_{OO} (black points). As seen, changes to σ_{OO} demonstrate the most structure. Also significant changes in the half-width are observed for changes made to σ_{HO} , with smaller changes coming from changes to ϵ_{HO} and ϵ_{OO} . Calculations were then made

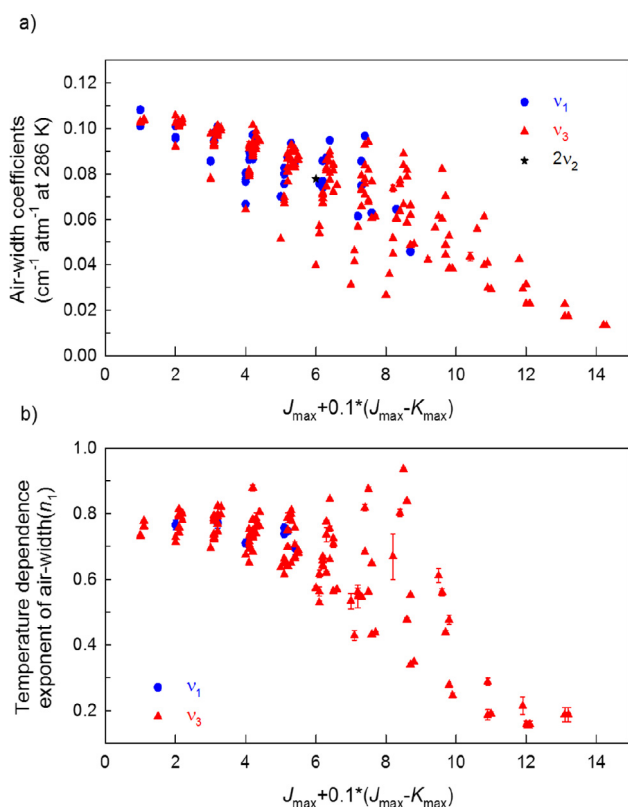


Fig. 6. (a) Measured air-broadened half-width coefficients for H₂O transitions in the ν_1 , ν_3 and $2\nu_2$ bands plotted as a function of $J_{\max} + 0.1 * (J_{\max} - K_{\max})$. (b) Measured temperature dependence exponents (n_1) of air-broadened half-width coefficients for H₂O transitions in the ν_1 and ν_3 bands plotted as a function of $J_{\max} + 0.1 * (J_{\max} - K_{\max})$. No temperature dependence exponent was measured for the weak transition in the $2\nu_2$ band. Where error bars are not visible, they are smaller than the symbol size.

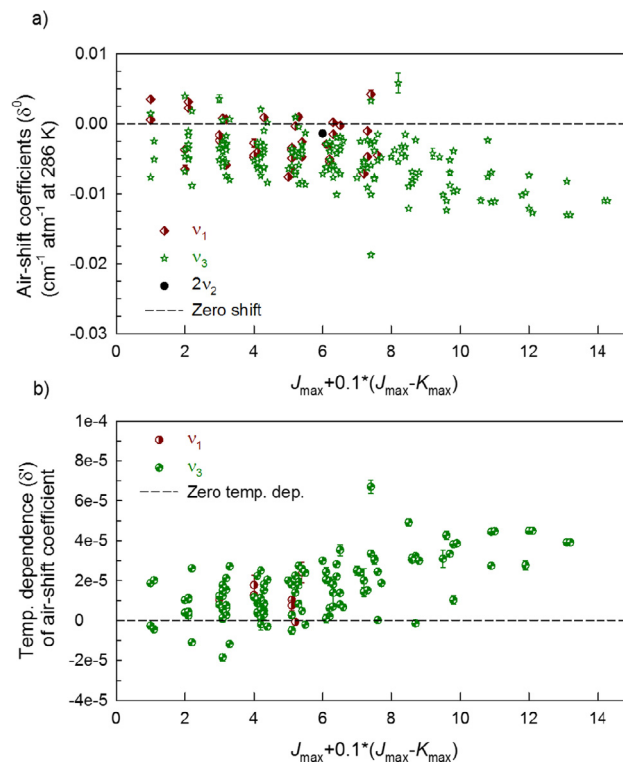


Fig. 7. (a) Measured air-shift coefficients $\delta^0(\text{air})$ for H₂O transitions in the ν_1 , ν_3 and $2\nu_2$ bands plotted as a function of $J_{\max} + 0.1 * (J_{\max} - K_{\max})$. (b) Measured temperature dependence ($\delta^0(\text{air})$) of air-shift coefficients for H₂O transitions in the ν_1 and ν_3 bands plotted as a function of $J_{\max} + 0.1 * (J_{\max} - K_{\max})$. Because the transitions were weak, no temperature dependence of air-shift coefficients were measured for any transition in the $2\nu_2$ band. Results seen in (a) indicate that air-shift coefficients become more negative as J increases and, the trend seen in (b) shows that temperature dependences of air-shift coefficients increase and become more positive with J .

by adjusting the atom-atom parameters and comparing the calculated half-widths with the 325 measured ν_2 transitions. In total 12 runs were made. The results from pot 11 gave the best agreement with the measurements. The final atom-atom parameters are $\epsilon_{\text{HO}} = 24.13$, $\epsilon_{\text{OO}} = 54.32$, $\sigma_{\text{HO}} = 2.42$, and $\sigma_{\text{OO}} = 3.16$, (0%, -5.0%, 15.0%, -4.98% change from pot 0, respectively). These changes in the atom-atom parameters are well within the uncertainty in the combination rule values.

To make the needed calculations, the present measured line list was taken and the rotational transitions for each vibrational band were extracted. The line list has 48,978 transitions broken down into 45 vibrational bands ranging from 1 rotational transition ($100 \leftarrow 020$) to 2551 rotational transitions ($010 \leftarrow 000$). There are too many transitions to make vibrationally dependent calculations for all transitions. The vibrational states were ignored and all unique rotational transitions were extracted for input into the line shape codes. This procedure produced a list of 5677 transitions. MCRB calculations were made for these transitions with ν_2 selected as the vibrational band, since there are more ν_2 lines in the list than any other band. In addition, vibrationally dependent calculations were made for the 224, 86, 2, and 3 transitions of ν_3 , ν_1 , $2\nu_2$, and $\nu_2 + \nu_3 - \nu_2$, respectively, that are measured in this work. Calculations of the half-width and line shift were made for N_2 -, O_2 -, and self-broadening at 7 temperatures: 200, 225, 275, 296, 350, 500, and 700 K.

The N_2 - and O_2 -broadening data were used to compute air-broadening by the usual formula

$$\gamma_{\text{air}} = 0.79\gamma_{\text{N}_2} + 0.21\gamma_{\text{O}_2} \quad (6)$$

at the seven temperatures of the study. With the air- and self-broadened data the temperature dependence of the half-width coefficient was determined using the power law

$$\gamma(T) = \gamma(T_{\text{ref}}) \left(\frac{T_{\text{ref}}}{T} \right)^n \quad (7)$$

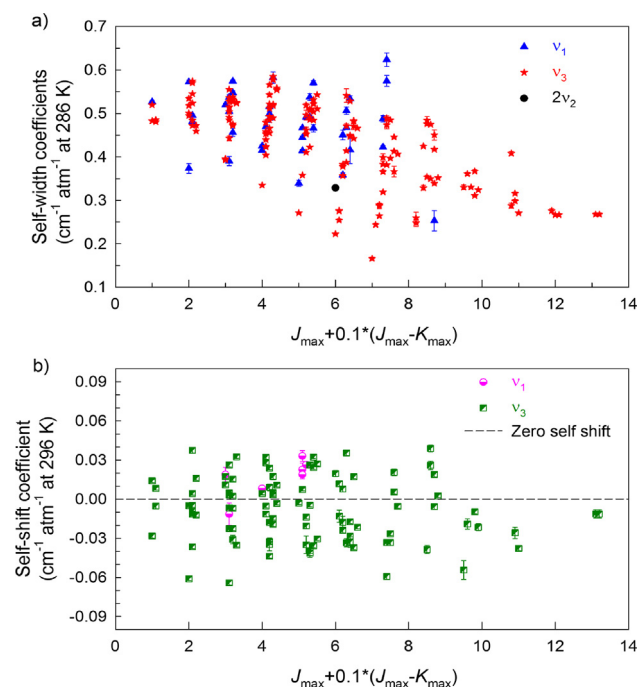


Fig. 8. (a) Measured self-width coefficients b_l^0 (self) for H_2O transitions in the ν_1 , ν_3 and $2\nu_2$ bands plotted as a function of $J_{\text{max}} + 0.1 * (J_{\text{max}} - K_{\text{max}})$. (b) Measured self-shift coefficients δ^0 (self) for H_2O transitions in the ν_1 and ν_3 bands plotted as a function of $J_{\text{max}} + 0.1 * (J_{\text{max}} - K_{\text{max}})$. No self-shift coefficient was measured for the single weak transition in the $2\nu_2$ band. Where error bars are not visible, they are smaller than the symbol size.

In Eq. (9), T_{ref} was taken to be 296 K and the temperature range of the fit was the 5 values from 200 to 350 K to be appropriate to Earth's atmosphere. It should be noted that a number of the calculated temperature exponents, n , are negative. Negative temperature dependence exponents were predicted theoretically by Hartmann et al. [66] and confirmed by theory [20] and experiment [20,21] by others. Here, these transitions correspond to the oblate limit ($K_a \sim 0$); however looking at the fits to the data using Eq. (9) it is apparent that the power law does not work well for these transitions.

Fig. 5A gives an example of the calculation of the temperature-dependence of the air-broadened half-width coefficient for a single transition in the ν_3 band, where the "data points" here are calculated values based on Eq. (8), and the n exponent corresponds to the slope of the line best fit to these points.

5. Results

5.1. Lorentz air-broadened half-width and temperature dependence exponent

The measured air-broadened half-width coefficients (converted to room temperature values of $T = 296$ K) for the H_2O transitions in the ν_1 , ν_3 and $2\nu_2$ bands are plotted as a function of $J_{\text{max}} + 0.1 * (J_{\text{max}} - K_{\text{max}})$ in Fig. 6(a) (J_{max} and K_{max} refer to the larger of the two J and K_a quantum numbers of the upper and lower rotational states of each transition involved). Different font symbols and colors are chosen to distinguish the data points for the three bands. Most of the measurements were made for the ν_3 band, and, while a few air-width coefficients were measured for the ν_1 band, only a

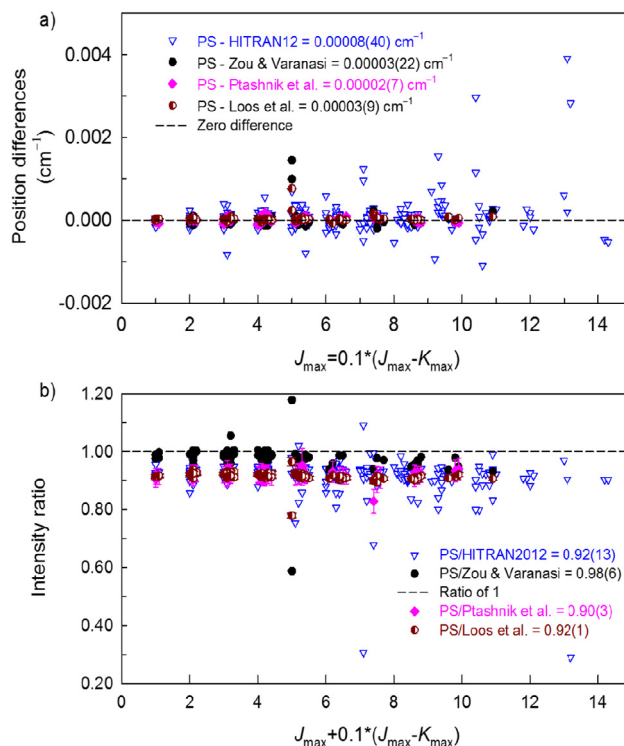


Fig. 9. (a) Line position differences for ν_3 band transitions that are common to the present study and HITRAN2012 [2], Zou and Varanasi [15], Ptashnik et al. [26] and Loos et al. [27,28] are plotted vs. $J_{\text{max}} + 0.1 * (J_{\text{max}} - K_{\text{max}})$. (b) Ratios of line intensities for the ν_3 band transitions that are common to this study and HITRAN2012 [2], Zou and Varanasi [15], Ptashnik et al. [26], and Loos et al. [27,28] vs. $J_{\text{max}} + 0.1 * (J_{\text{max}} - K_{\text{max}})$ are plotted. The means and standard deviations of the differences and ratios compared are listed in the legends of the relevant panels (a) and (b).

single air-broadened half-width coefficient was measured in the weak $2\nu_2$ band. Consistent with previous measurements and calculations [7–35], Fig. 6(a), illustrates that the air-broadened H_2O half-width coefficients for the same K_{\max} value generally decrease with increasing J_{\max} . For a fixed J_{\max} value, the air-broadened half width increases with K_{\max} to a local maximum, and then decreases with increasing K_{\max} . For $J_{\max} = 1-8$, air-width coefficients were measured for all possible K_{\max} values (up to $K_{\max} = J_{\max}$), but for higher J_{\max} values air-widths were obtained for a smaller range of K_{\max} . Similar trends are seen in Fig. 6(b) where the temperature dependence exponents of air-broadened half-width coefficients (n_1) vs. $J_{\max} + 0.1 * (J_{\max} - K_{\max})$ are shown. Because of the weakness of the single $2\nu_2$ transition, although its room temperature half-width coefficient was measured, it was not possible to retrieve a reliable temperature dependence exponent and hence its value was fixed to that in HITRAN2012 [2]. The measured air-width coefficients range approximately between 0.02 and 0.11 $\text{cm}^{-1} \text{atm}^{-1}$ at 296 K, and the temperature dependence exponents of air-broadened half-width coefficients vary between 0.1 and ~ 1.0 . Uncertainties associated with the measurements are plotted in the figure, and where error bars are not visible, their values are smaller than the size of the symbols used.

5.2. Air-shift coefficients and their temperature dependence

The variations of the measured air-shift coefficients and their temperature dependences are shown in Fig. 7. In the top panel (a), the measured air-shift coefficients, $\delta^0(\text{air})$, for transitions in the ν_1 , ν_3 and $2\nu_2$ bands are plotted as a function of $J_{\max} + 0.1 * (J_{\max} - K_{\max})$ and, in (b) the measured temperature dependences (δ'_{air}) of the air-shift coefficients in the ν_1 and ν_3 bands are also shown as a function of $J_{\max} + 0.1 * (J_{\max} - K_{\max})$. Because the $2\nu_2$ transitions were weak in our spectra, although the air-shift coefficient was measured for one transition, no temperature dependence of the air-shift coefficient could be determined. The measurements plotted in (a) indicate that the air-shift coefficients become more negative as J increases and, the trend seen in (b) shows that temperature dependences of the measured air-shift coefficients have smaller (and some negative) values for low J , and they become larger and more positive with increasing J . In panels (a) and (b), the horizontal dashed line corresponds to zero air-shift coefficient and zero temperature dependence of air-shift coefficient, respectively. Similar to Fig. 6, different symbols and colors are used in Fig. 7 to distinguish transitions from the various bands. The majority of the measured air-shift coefficients vary from nearly $+0.005$ to $-0.013 \text{ cm}^{-1} \text{atm}^{-1}$ at 296 K and the temperature dependence coefficients of air-shifts vary nearly in the -2×10^{-5} to $+5 \times 10^{-5} \text{ cm}^{-1} \text{atm}^{-1} \text{K}^{-1}$ range, respectively. Uncertainties associated with the measurements are plotted and where error bars are not visible, their values are smaller than the size of the plot symbols used.

5.3. Self-width and self-shift coefficients

Since no spectra of pure water vapor at higher temperatures were included in the present analysis, only room-temperature values for the self-width and self-shift coefficients could be obtained. Self-width and self-shift coefficients were measured for 209 and 106 transitions, respectively (see Table 2). The measured self-width coefficients in the ν_1 , ν_3 and $2\nu_2$ bands plotted as a function of $J_{\max} + 0.1 * (J_{\max} - K_{\max})$ are displayed in Fig. 8(a). The measured self-shift coefficients in the ν_1 and ν_3 bands plotted as a function of $J_{\max} + 0.1 * (J_{\max} - K_{\max})$ are shown in Fig. 8(b). No self-shift coefficient was measured for the weak transition in the $2\nu_2$ band. It is seen in (a) that, as for the air-widths, the self-width coefficients

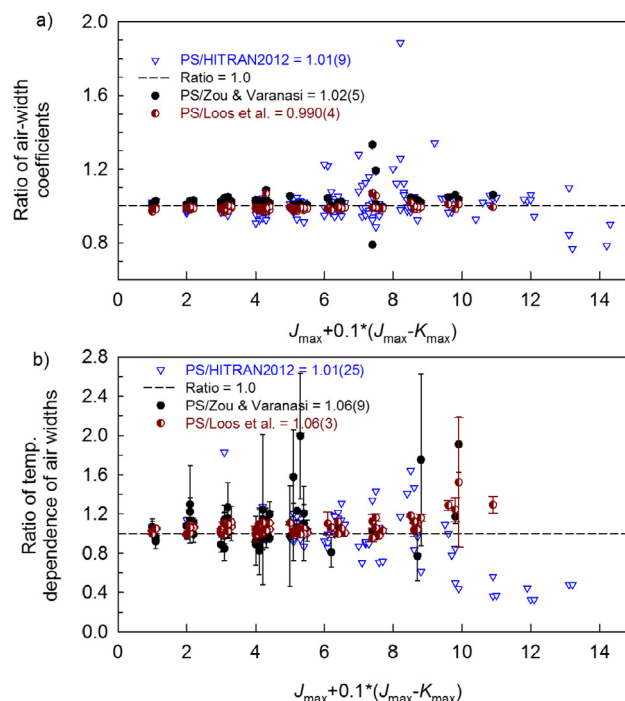


Fig. 10. Comparisons of present air-broadened half-width coefficients and their temperature dependence exponents with HITRAN2012 [2], Zou and Varanasi [15], and Loos et al. [27] are plotted as a function of $J_{\max} + 0.1 * (J_{\max} - K_{\max})$. (a) The ratios of air-broadened half-width coefficients (PS/Other studies). (b) The ratios of the temperature dependence exponents of air-broadened half-width coefficients (PS/Other). In both panels the mean and standard deviation of each set of ratios are given in the legend. Uncertainties associated with the measurements are represented by error bars in the plots for PS/Zou and Varanasi and for PS/Loos et al. Where error bars are not visible, they are smaller than the size of the symbol used.

generally decrease with increasing J_{\max} . However, the magnitudes of the self-widths are much larger; the self-width coefficient values range from 0.15 to more than 0.6 $\text{cm}^{-1} \text{atm}^{-1}$ at 296 K, while the largest measured air-width is $\sim 0.11 \text{ cm}^{-1} \text{atm}^{-1}$ at 296 K. The self-shift coefficients plotted in (b) show variations with K and J quantum numbers that are somewhat different from those for air-shifts of the same transitions (see Fig. 7), and the magnitudes of the self-shifts are larger than those observed for air-shifts. The measured self-shift coefficients have both positive and negative values varying between $+0.05 \text{ cm}^{-1} \text{atm}^{-1}$ and $-0.06 \text{ cm}^{-1} \text{atm}^{-1}$ at 296 K.

6. Comparison of measured and calculated line parameters

In this section, comparisons of the present measured line parameters are made first with measurements reported in the literature. Among the large number of measurements that are available for the various bands of H_2O , only a few are directly comparable with the present study of air- and self-broadened line shapes in the ν_1 , ν_3 and $2\nu_2$ bands. Most other H_2O studies available in the literature were related to different spectral regions, different perturbing gases (such as O_2 , N_2 , and H_2), made only very few measurements, or used different types of recording instruments (e.g., diode laser spectrometer system) in obtaining the data. Our comparisons are therefore limited to results from three similar experimental studies (where spectra were obtained using high-resolution FTS) even though different experimental and analysis procedures were followed in each study and some of the many line parameters measured in each study varied from the present work [15,26–28]. We also compare our results and those of Refs. [15,26–28] with values reported in

the HITRAN2012 database [2], which in the ν_1 and ν_3 region are largely the results of Ref. [4]. Finally, the measured values from PS are compared to present study MCRB calculated values.

6.1. Comparison of line positions and intensities

In Fig. 9(a) and (b), comparisons of line positions and intensities between present measurements, measurements from Refs. [15,26–28], and the initial input values from HITRAN2012 database [2] are shown. The line positions and intensities in the present study MCRB calculations are the same as in Ref. [2] and therefore the differences in line positions or the intensities between this study and the MCRB calculated list are not considered. In panel (a) the line position differences: (PS–HITRAN2012), (PS–Zou & Varanasi), (PS–Ptashnik et al.), and (PS–Loos et al.) vs. $J_{\max} + 0.1 * (J_{\max} - K_{\max})$ are plotted. The means and standard deviations of the differences for the above cases are $+0.00006 \pm 0.00040 \text{ cm}^{-1}$, $+0.00003 \pm 0.00022 \text{ cm}^{-1}$, $+0.00002 \pm 0.00007 \text{ cm}^{-1}$ and $+0.00003 \pm 0.00009 \text{ cm}^{-1}$, respectively. The number of reported line positions compared to present measurements is different in each of the four cases. While all the 313 line positions measured in the present study are compared with HITRAN2012 [2], the comparisons with the other laboratory studies [15,26–28] are limited to the 82 ν_3 transitions reported in Table 3 for which the present study measured the full set of nine spectroscopic parameters; this means that the PS had 76 transitions in common with Zou and Varanasi [15], 61 with Ptashnik et al. [26], and 82 with Loos et al. [27,28]. Even if we limit the J values up to 11 (see Fig. 9(a)), the largest scatter is observed between PS and HITRAN2012 [2]. The two black solid circles displaying the largest scatter in (PS – Zou and Varanasi) correspond to the two close doublet transitions $5\ 5\ 1 \leftarrow 5\ 5\ 0$ and $5\ 5$

$0 \leftarrow 5\ 5\ 1$ located at 3726.6171 and $3726.6255 \text{ cm}^{-1}$, respectively. Overall, all position differences (except for HITRAN2012) agree to within $\pm 0.0001 \text{ cm}^{-1}$. The large scatter in position differences seen between PS and HITRAN2012 compared to other studies is attributed to comparisons with all measured lines (strong and weak) with HITRAN versus only the strong lines compared in other studies. We note that some of the HITRAN2012 line positions, particularly for transitions at higher rotational quantum numbers, may be calculated rather than measured values (see Fig. 2 of Ref. [2]).

The comparisons shown in Fig. 9(b) indicate that the closest agreement of line intensities is between the PS and Zou and Varanasi [15] with a mean and standard deviation of (PS/Zou and Varanasi) = 0.98 ± 0.06 . The means and standard deviations of the other three intensity ratios; (PS/HITRAN2012), (PS/Ptashnik et al.) and (PS/Loos et al.) are 0.92 ± 0.13 , 0.90 ± 0.03 and 0.92 ± 0.01 , respectively, indicating our present intensities are lower by 8–10%. There are no plausible explanations for us to offer for these rather large systematic differences between present measurements and those in Refs. [26,27] except for the fact that there are several differences among the individual experimental setups concerning sample gas containment, type of spectra (e.g., only H_2O , $\text{H}_2\text{O} + \text{air}$ or both) analyzed, whether the spectra were taken only at room temperature [15] or at different temperatures, and which spectral line parameters were measured in the analyses and how the analyses were performed. Larger absorption path lengths available in Ref. [26,27] allowed those authors to measure positions and intensities for a much larger number of transitions compared to the PS, while in Refs. [15,26], the absorption path lengths used for self-broadened spectra in the $2.7 \mu\text{m}$ region were shorter than those used in the PS.

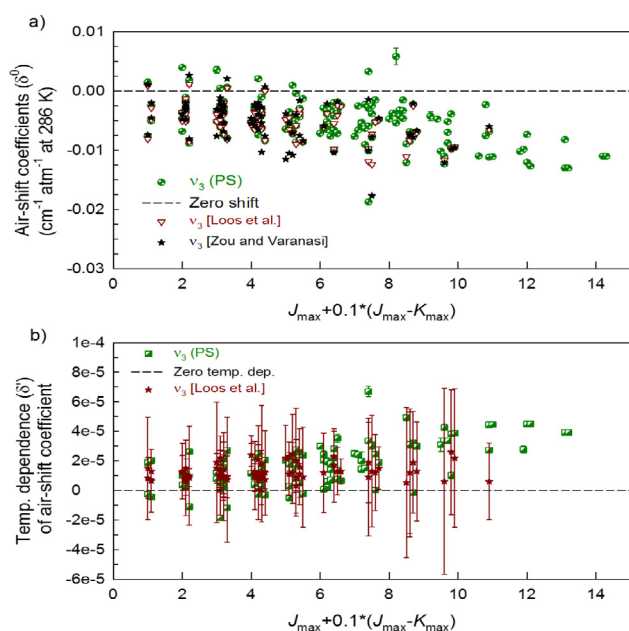


Fig. 11. Comparison of air-shift coefficients and their temperature dependences are shown for transitions in the ν_3 band of H_2O . (a) Air-shift coefficients δ^0 (in $\text{cm}^{-1} \text{ atm}^{-1}$ at 296 K) determined from PS, Zou and Varanasi [15], and Loos et al. [27] are plotted vs. $J_{\max} + 0.1 * (J_{\max} - K_{\max})$. (b) Temperature dependences of air-shift coefficients δ' (in $\text{cm}^{-1} \text{ atm}^{-1} \text{ K}^{-1}$) from PS and Loos et al. [27] are plotted vs. $J_{\max} + 0.1 * (J_{\max} - K_{\max})$. There are no temperature dependences of air-shift coefficients reported by Zou and Varanasi [15] available for comparison. In both panels uncertainties of the measured values are represented by error bars of the same color as the symbol; where error bars are not visible they are smaller than the symbol size.

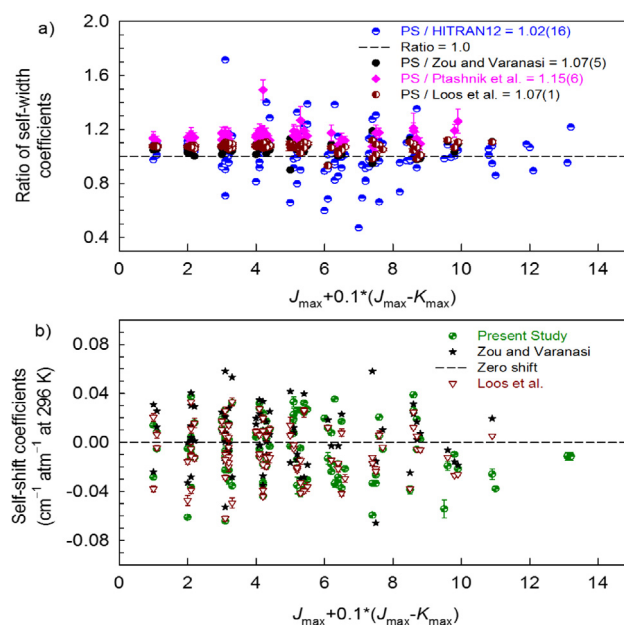


Fig. 12. Comparison of self-broadened half-width and self-shift coefficients from PS and HITRAN2012 [2], Zou and Varanasi [15], Ptashnik et al. [26], and Loos et al. [28] for transitions in the ν_1 and ν_3 bands of H_2O plotted as a function of $J_{\max} + 0.1 * (J_{\max} - K_{\max})$. (a) Ratios of self-broadened half-width coefficients. Means and standard deviations of the width ratios are given in the legend, where the standard deviation is given in parentheses in units of the last digit quoted. (b) Self-shift coefficients from PS, Zou and Varanasi, and Loos et al. are overlaid and show similar variations with $J_{\max} + 0.1 * (J_{\max} - K_{\max})$. HITRAN2012 and Ptashnik et al. do not report self-shift coefficients. In both panels, except for HITRAN2012 widths where errors were not taken into account, where no error bars are visible, the uncertainties are smaller than the symbol size used.

6.2. Comparison of air-width coefficients and their temperature dependence exponents

Comparisons of present measured air-broadened half-width coefficients and their temperature dependence exponents with HITRAN2012 [2], Zou and Varanasi [15], and Loos et al. [27] as a function of $J_{\max} + 0.1 * (J_{\max} - K_{\max})$ are plotted in Fig. 10(a). The means and standard deviations of the ratios of air-broadened half-width coefficients are: PS/HITRAN2012 = 1.01 ± 0.09 , PS/Zou and Varanasi = 1.02 ± 0.05 , and PS/Loos et al. = 0.990 ± 0.004 . In general, comparison with the HITRAN2012 database shows slightly larger scatter than the other two measured values (all PS measured values are compared with HITRAN2012). Error bars representing uncertainties associated with the measurements are included in the plots for PS/Zou and Varanasi and PS/Loos et al. Where error bars are not visible, they are smaller than the size of the symbol used. Uncertainties based upon error codes listed for HITRAN2012 values were not taken into consideration in making these plots. As discussed in Section 2.1.5 of Ref. [2], the set of HITRAN2012 air-broadened half width coefficients contains both measured and calculated values.

The ratios of the temperature dependence exponents for the air width coefficients vs. $J_{\max} + 0.1 * (J_{\max} - K_{\max})$ are plotted in Fig. 10(b). As in Fig. 10(a) larger differences between the present measurements and HITRAN2012 are seen, especially for $J_{\max} > 6$, while except for a few outliers, agreement is closer with the Zou and Varanasi and the Loos et al. measurements. The means and standard deviations of the temperature dependence exponents of air-broadened half-width coefficients for PS/HITRAN2012 = 1.01 ± 0.25 , PS/Zou and Varanasi = 1.06 ± 0.09 , and PS/Loos et al. = 1.06 ± 0.03 . Uncertainties in the measurements are shown as error bars only for PS/Zou and Varanasi and the PS/Loos et al. ratios. The larger uncertainties in the ratios for PS/Zou and Varanasi are attributed to the larger uncertainties associated with the temperature

dependence exponents reported in Ref. [15]. As in Fig. 10(a) uncertainties corresponding to the error codes for the HITRAN2012 values are not considered in the present plots.

6.3. Comparison of air-shift coefficients and their temperature dependences

Comparisons of air-shift coefficients δ^0 and the temperature dependence of air-shift coefficients δ' for the ν_3 transitions of H_2O are plotted in Fig. 11. In the top panel (a), the experimentally-determined air-shift coefficients from the PS, the Zou and Varanasi [15], and the Loos et al. [27] studies are plotted vs. $J_{\max} + 0.1 * (J_{\max} - K_{\max})$. The air-shift coefficients become more negative with increasing J and the shift coefficients vary approximately between $+0.005$ and $-0.018 \text{ cm}^{-1} \text{ atm}^{-1}$ at 296 K. Because of the smaller magnitude of the air-shift coefficients compared to air-width coefficients, we have plotted and overlaid the measured air-shift coefficients rather than ratios or differences between the air-shift coefficients measured for the same transitions. In Fig. 11 (b), similarly the experimentally-determined temperature dependences of air-shift coefficients (in $\text{cm}^{-1} \text{ atm}^{-1} \text{ K}^{-1}$) from the PS and Loos et al. [27] are plotted as a function of $J_{\max} + 0.1 * (J_{\max} - K_{\max})$. Temperature dependences of air-shifts were not reported by Zou and Varanasi [15]. In both panels (a) and (b) measurement uncertainties are represented by error bars, and where no error bars are visible, the measured uncertainties are smaller than the size of the symbols used. For the air-shift coefficients, the uncertainties in all three sets of measurements are small. It is clearly seen from Fig. 11(a) and (b) that as the air-shift coefficients change sign from positive to negative and become more negative with increasing J , their temperature dependence coefficients become more positive with increasing J , and the small negative values seen for some low- J transitions are not present at higher J values.

6.4. Comparison of self-width and self-shift coefficients

Self-broadened half-width coefficients from four separate measurements and self-shift coefficients from three different experiments are compared in Fig. 12. Although several other experimental measurements of self-width and self-shift coefficients have been reported in the literature (e.g., Refs. [7,10]), there are not many measurements outside of Refs. [15,26,28] for the same transitions in common with the present study. The ratios of self-width coefficients: PS/HITRAN2012, PS/Zou and Varanasi, PS/Ptashnik et al. and PS/Loos et al. as a function of $J_{\max} + 0.1 * (J_{\max} - K_{\max})$ are plotted in the top panel (a). There are more transitions compared and more scatter with HITRAN2012 than with other studies. The means and standard deviations of the ratios of the self-width coefficients are: PS/HITRAN2012 = 1.02 ± 0.16 , PS/Zou and Varanasi = 1.07 ± 0.05 , PS/Ptashnik et al. = 1.15 ± 0.06 , (PS/Loos et al.) = 1.07 ± 0.01 . Except for the PS/HITRAN2012 ratios, uncertainties associated with the measurements are included in the plots. Where no error bars are visible, the uncertainties are smaller than the symbol size used. The horizontal dashed line represents a ratio of unity.

The measured self-shift coefficients from PS, Zou and Varanasi, and Loos et al. with the corresponding uncertainties as a function of $J_{\max} + 0.1 * (J_{\max} - K_{\max})$ are plotted in Fig. 12(b). The self-shift coefficients in general range within $\pm 0.07 \text{ cm}^{-1} \text{ atm}^{-1}$ at 296 K and similar variations with J_{\max} and K_{\max} are seen in all three sets of measurements. No self-shift coefficients were reported by Ptashnik et al. or in HITRAN2012. Where no error bars are visible, the uncertainties are smaller than the symbol size used. The horizontal dashed line corresponds to zero shift coefficients.

The measured values and the MCRB calculated values (both from PS) for the air-broadened half-width and pressure shift

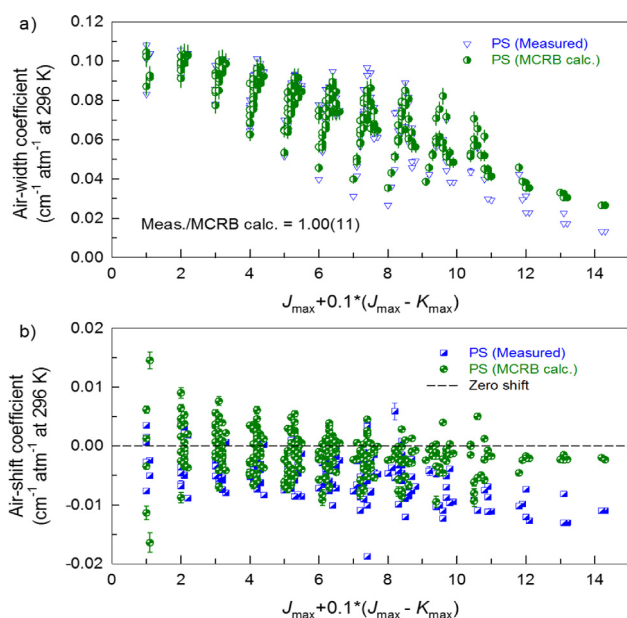


Fig. 13. (a) Measured (blue) and MCRB calculated (green) air-broadened H_2^{16}O (H_2^{16}O -air) Lorentz half-width coefficients plotted vs. $J_{\max} + 0.1 * (J_{\max} - K_{\max})$. The mean and standard deviation (on panel (a) in parentheses in units of the last digit quoted) of the ratio of measured to calculated half-width coefficients is 1.00 ± 0.11 . (b) Measured (blue) and calculated (green) H_2^{16}O -air pressure-shift coefficients plotted vs. $J_{\max} + 0.1 * (J_{\max} - K_{\max})$. No differences between measurements and calculations of air-shift coefficients are computed or plotted. (For interpretation of the references to color in this figure legend, the reader is referred to the web version of this article.)

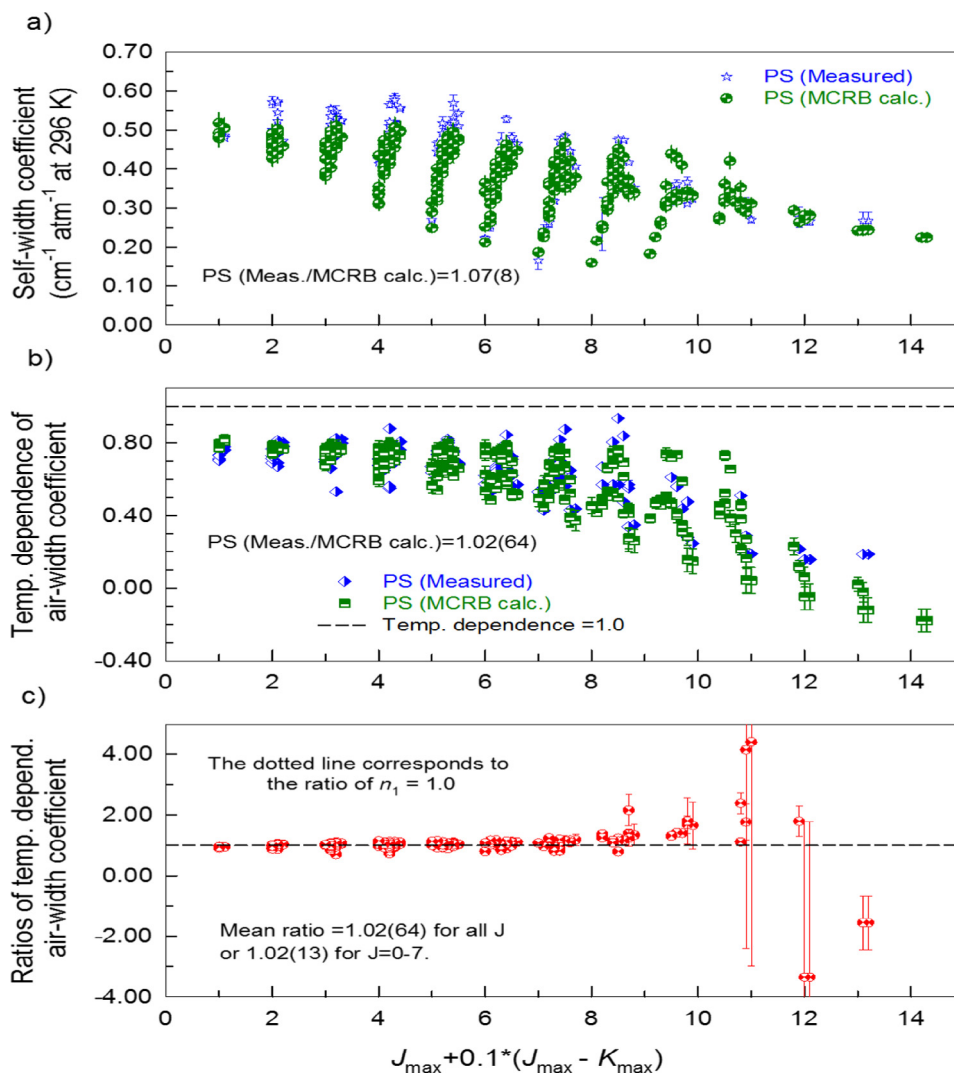


Fig. 14. (a) Measured (blue) and MCRB calculated (green) Lorentz self-broadened half-width coefficients plotted vs. $J_{\max} + 0.1 * (J_{\max} - K_{\max})$; the mean and standard deviation (on the figure in parentheses in units of the last digit quoted) of the ratio of measured to calculated self-width coefficients is 1.07 ± 0.08 . (b) Measured (blue) and MCRB calculated (green) temperature dependence exponents (n_1) of air-broadened half width coefficients of H_2^{16}O -air plotted vs. $J_{\max} + 0.1 * (J_{\max} - K_{\max})$ with the mean (and standard deviation) of measured to calculated n_1 as 1.02 ± 0.64 . (c) The same information in (b) except the ratios of n_1 are plotted vs. $J_{\max} + 0.1 * (J_{\max} - K_{\max})$. The mean (with standard deviation) of the ratios is 1.02 ± 0.64 when ratios for all J values are averaged. The mean ratio with the standard deviation is 1.02 ± 0.13 when n_1 values for only $J \leq 7$ are considered. (For interpretation of the references to color in this figure legend, the reader is referred to the web version of this article.)

coefficients, temperature dependence exponents of air-broadened half-width coefficients and, the room-temperature self-broadened half-width and self-shift coefficients are plotted in Figs. 13 and 14. All parameters are plotted versus $J_{\max} + 0.1 * (J_{\max} - K_{\max})$. It is apparent in the figures that the measured and calculated line shape parameters are in very good agreement for $J_{\max} \leq 8$, but the differences are larger for higher values of J_{\max} (see, for example, Fig. 14(c)).

7. Uncertainties in the measured parameters

It is important to know how these uncertainties vary in the Lorentz half-width and pressure shift coefficients at the reference temperature, $T_0 = 296$ K. However, it is equally if not more important to know how these uncertainties propagate to the temperature and volume mixing ratio conditions in spectral simulations. As pointed out in our earlier study of the temperature dependence of air-broadened line shape parameters in CO_2 [67] and the recent measurements of HDO-CO_2 line shape parameters [44], when one uses a half-width coefficient determined at 296 K and its tempera-

ture dependence exponent (if not determined from the same study) from a different source such as HITRAN [1,2], it is generally assumed that the half-width coefficients at 296 K are the best determined values and the uncertainty in the temperature dependence of the half-width coefficient as the temperature gets farther from 296 K. It has been shown [67] that, for each line, the experimental values of the two half-width and the two pressure-shift parameters (at two temperatures) are highly correlated and the uncertainties as a function of temperature are quite different (e.g., see Figs. 7 and 8 in [67] and Figs. 12 and 13 in [44]). It was discussed [44,67] that because of the large number of spectra included in the least squares solution, the uncertainties in the retrieved parameters are very small and there are various other problems associated with the fits that dominate the actual uncertainties. These include uncertainties in the measurement of gas conditions (pressure, temperature and volume mixing ratios etc.), uncertainties in the spectral line shapes assumed in the measurements, and modeling of the spectral line parameters used. In particular there was no effort made in the PS to model separately the speed

dependences of self- and foreign-gas broadening and pressure shift or the temperature dependence of the speed dependence. Each of these parameters may have only a small effect upon the overall solution. While the speed dependence model applied in the PS represents all temperatures, the model is unlikely to hold rigorously for all collisional speeds. Although we were aware of these effects, our fitting software did not include some of these finer details and we did not observe any fit residuals above the noise levels of the individual spectra in the final multispectrum fittings. These considerations have to be kept in mind while the absolute errors in our present measurements are discussed below.

In the PS, by fitting all experimental spectra obtained with two different absorption cells and sample gases of different pressures and volume mixing ratios at various temperatures simultaneously, the uncertainties due to random errors in the various retrieved parameters are minimized as illustrated in several figures (e.g., Figs. 3 and 4). The absorption path lengths of the two cells are known to $\leq 0.01\%$ while the sample pressures and temperatures are determined to $\pm 0.05\%$ and ± 0.2 K, respectively. Effects due to instrumental line shape distortion and residual phase errors were taken into consideration during the fitting process. Correlation coefficients between fitted parameters were internally computed in the multispectrum fitting software while uncertainties are calculated in the retrieved parameters. For example, correlation of each measured line position with every other adjusted parameters such as all other spectral line parameters, zero level, phase error, background polynomial fit coefficients and, a file of correlation matrix coefficients are constructed and available for each fitted interval. Without providing the correlation matrices for each of the fitted parameters, it is not possible to explain all of these details discussed above to compute the total uncertainties in each measured parameter. Prior calibration of wavelength scales of all spectra before starting the multispectrum fittings ensures the best and consistent results in the measurements of line positions and pressure-shift coefficients. Values listed in Table 3 and the comparisons made with all four other experimental measurements [2,15,26,27] in Fig. 9 suggest that for the best measured line positions, especially for the ν_3 band, the accuracy of the PS is thought to be of the order of ± 0.0001 cm^{-1} . The results given in Table 3 also suggest that the intensities of strong transitions for the ν_3 band are determined with very high precision in the PS on the order of 0.01–0.05%. Even if one assumes a 100 times the statistical measurement uncertainty, the absolute errors in the PS intensities should be well within 1–5%. However, comparisons with the calculated values [2] as well as two of the three experimental measurements [26,27] in Fig. 9(b) indicate that our intensities are lower by 8–10% than those values, while the measurements by Zou and Varanasi [15] show fairly good agreement ($98 \pm 0.08\%$). The PS Lorentz air- and self-broadened half-width and the pressure-shift coefficients are estimated to be accurate to ± 1 and $\pm 5\%$, respectively. Absolute accuracies in the measured temperature dependences of air-shift coefficients, off-diagonal relaxation matrix element coefficients and speed dependence parameters are difficult to assess but are estimated conservatively to be within 5–15% depending upon the J, K quanta of the individual transitions. It is useful here to briefly discuss the similarities and differences in the experimental procedures and analyses techniques used in the PS, Zou and Varanasi [15], Ptashnik et al. [26] and Loos et al. [27,28] experiments since our present measurements have been compared to these.

Zou and Varanasi [15] obtained their data in the 3000–4050 cm^{-1} region using a Bruker IFS-125HR FTS and spectra were obtained at three temperatures, $T = 252, 273$ and 296 K with absorption path lengths of 2.15 and 9.28 cm. Known amounts of sample mixtures were introduced and sealed within the gas cells. Self-broadened spectra were recorded only at $T = 296$ K. For air-broadening measurements, groups of spectra recorded at each of

the three temperatures were fitted simultaneously using a Voigt line shape profile and later the various results were combined to obtain the air- and self-broadening and pressure-shift coefficients and their temperature dependences. The retrieved parameters included line positions, intensities, and Lorentz broadening coefficients but no other parameters (such as line mixing or speed dependence) were reported. Ptashnik et al. [26] obtained their experimental spectra in the 3440–3970 cm^{-1} region using a Bruker IFS-120HR FTS that was upgraded to Bruker IFS-125HR FTS. A specially built short absorption cell of 4.78 mm long was employed to record two room temperature spectra at 294 K and the cell was filled with water vapor to desired pressures and allowed several hours (12 h) to reach equilibrium conditions before starting the data acquisition. Short spectral segments from both spectra were fitted individually using a Voigt line shape model along with collisional narrowing parameter applied in the analysis. Line positions, intensities, self-broadened half-width and Dicke narrowing parameters were retrieved for each fitted line. No other line parameters (such as the self-shift coefficients, temperature dependences of self-width and self-shift coefficients, line mixing, speed dependence) were reported. Loos et al. [27,28] reported their results in two separate publications; line positions, intensities and self-broadened line shapes in Ref. [28], and measurements of air-broadened line shape parameters in Ref. [27]. Their experimental set up consisted of a high resolution Bruker IFS-125HR FTS, and a large number of spectra were recorded at different spectral resolutions. Two absorption cells (one variable-path) that were cooled to 213 K and heated to 353 K were employed to obtain the spectra at absorption path lengths from 0.249 to 168.21 m. A large number of pure and air-broadened spectra were obtained at three different temperatures. The measurements in [27,28] were made using a constant flow of $\text{H}_2\text{O}/\text{air}$ mixtures through the cells unlike the other three experiments (including the PS) where sample mixtures were introduced into the gas absorption cells and sealed. Automated software chose the various micro-windows (extending from 0.25 to 0.75 cm^{-1}) to be fitted and spectra were fitted interactively. The retrieved line parameters included positions, intensities, air- and self-broadened half-width coefficients along with corresponding speed dependence parameters, collisional narrowing parameters, self- and air-shift coefficients, temperature dependences of pressure broadening and pressure shift coefficients, line mixing using the first order Rosenkranz approximation and their temperature dependence, when applicable. Different steps were used to measure all parameters and extensive error analyses of the various parameters were discussed. In the PS, although measurements were obtained using shorter cells than in Refs. [27,28], all spectra recorded at various experimental conditions were fitted simultaneously in much larger spectral intervals, thus providing a single consistent set of results for all measured parameters.

8. Summary, conclusions, and future studies

The present study involved simultaneous analysis of 18 high-resolution (0.006 and 0.008 cm^{-1}), high signal-to-noise ratio ($>1500:1$) Fourier transform spectra of pure and air-broadened H_2^{16}O in the 3645–3980 cm^{-1} spectral region. The spectra were recorded at the Pacific Northwest National Laboratory (PNNL) in Richland, Washington using two absorption cells that are both coolable as well as heatable with path lengths of 9.906(1) and 19.95(1) cm. Spectra of H_2O -air mixtures at different volume mixing ratios of H_2O were obtained at 268, 296 and 353 K. All 18 experimental spectra were fitted simultaneously applying an interactive multispectrum fitting technique whereby a consistent set of line parameters were retrieved. We have measured air-broadened half-width and pressure shift coefficients and their temperature

dependences for several strong transitions in the ν_3 and ν_1 bands of H_2^{16}O . Room-temperature air-width and air-shift coefficients were measured for over 200 transitions, while the temperature dependences of air-width and air-shift coefficients were obtained for only over 100 transitions. The majority of those measurements were for the stronger transitions in the ν_3 band. In addition, we also measured room-temperature self-width and self-shift coefficients for nearly the same number of transitions as for room temperature air-width and air-shift coefficients. For the analysis, a non-Voigt line shape profile was employed by including speed dependence and collisional line mixing via off-diagonal relaxation matrix elements, when appropriate. Line positions and line intensities were measured for over 300 transitions, and the full set of line shape parameters was measured for 92 of these transitions. Line mixing parameters were determined for 12 pairs of transitions in the ν_3 band. The measured line shape parameters compare well with other recent measurements of similar nature [15,26–28] as well as with values available in the HITRAN2012 database [2].

Even though non-Voigt line shapes were applied to the present measurements, future investigations to include improved line shape modifications suggested by Ngo et al. [68,69] and Tran et al. [70,71] could be undertaken. Additional modifications including separate speed dependence and temperature dependences of speed dependence for the broadening and pressure-shift coefficients as suggested in several recent studies should be examined. Similarly, the speed dependence of the parameter and its relationship to its temperature dependence should be addressed separately in both the self- and foreign-gas broadened measurements. The implementation of these new line parameters could not be achieved in the present study because of the limitation in our fitting software. It should, however, be noted that there were no residuals beyond the noise level of our spectra in our multispectrum fittings to improve the solution other than the fact that one could employ more sophisticated line shape functions. Tran et al. [22] discussed the effects of velocity on the shapes of six $R(J)$ transitions of the ν_3 band water vapor broadened with N_2 . The authors demonstrated that using the Voigt profile alone could not provide satisfactory results even though at higher pressures Dicke narrowing and Doppler effects were negligible. In their study [22], the authors used velocity-dependent broadening and shift coefficients and concluded that all profiles, regardless of pressures and of the transition can be correctly modeled using a single set of memory parameters. For more details, the reader is directed to the original article [22]. We would like to point out that residuals consistent with collisional narrowing (Dicke narrowing) were observed in our low pressure spectra, but when high pressure spectra were added to the solution, we were not able to retrieve reliable values for both collisional narrowing and speed dependence parameters. We found that speed dependence parameters were more significant when high-pressure, high S/N ratio spectra were included in the simultaneous fits.

In addition to the measurements in the present study, line shape parameters for transitions in the fitted interval (3645–3975 cm^{-1}) have been calculated using the modified complex Robert-Bonamy formalism (MCRB). Line positions and intensities in the MCRB list were taken from HITRAN2012. The measured values for self- and air-broadened widths, air-shifts, and the temperature-dependences of the air-widths compare very well with our present MCRB calculations, with the best agreement obtained for transitions with $J_{\text{max}} \leq 8$.

Acknowledgments

Cooperative agreements and contracts with National Aeronautics and Space Administration have supported the research performed at the College of William and Mary and at NASA Langley

Research Center through the Upper Atmosphere Research Program and the AQUA Validation Program. Research performed at the University of Massachusetts Lowell is supported by the National Science Foundation through Grant No. AGS-1622676. The Department of Energy's Office of Biological and Environmental Research located at the Pacific Northwest National Laboratory (PNNL) supported part of this research. PNNL is operated for the United States Department of Energy by Battelle under contact No. DE-AC06-76RLO 1830.

Appendix A. Supplementary material

The descriptions of the various parameters listed under different columns in the Supplemental file are provided with appropriate header information and footnotes at the bottom of the file. Only those transitions for which at least one parameter value was adjusted in the multispectrum fit are included in this file. If any parameter value of a transition was held fixed in the least squares fit, its value is indicated as 0.0 or Fixed in the Supplemental file. Supplemental material associated with this article can be found in the online version of this manuscript. A complete list of all calculated spectral line parameters of water vapor transitions in the 1100–4100 cm^{-1} region using the MCRB formalism is available at http://faculty.uml.edu/Robert_Gamache. Supplementary data associated with this article can be found, in the online version, at <https://doi.org/10.1016/j.jms.2017.11.011>.

References

- [1] I.E. Gordon, L.S. Rothman, C. Hill, R.V. Kochanov, Y. Tan, P.F. Bernath, M. Birk, V. Boudon, A. Campargue, K.V. Chance, B.J. Drouin, J.-M. Flaud, R.R. Gamache, D. Jacquemart, V.I. Perevalov, A. Perrin, M.-A.H. Smith, J. Tennyson, H. Tran, V.G. Tyuterev, G.C. Toon, J.T. Hodges, K.P. Shine, A. Barbe, A. Csaszar, M.V. Devi, T. Furtenbacher, J.J. Harrison, A. Jolly, T. Johnson, T. Karman, I. Kleiner, A. Kyuberis, J. Loos, O. Lyulin, S.N. Mikhailenko, N. Moazzen-Ahmadi, H.S.P. Müller, O. Naumenko, A. Nikitin, O. Polyansky, M. Rey, M. Rotger, S. Sharpe, K. Sung, E. Starikova, S.A. Tashkun, J.V. Auwera, G. Wagner, J. Wilzewski, P. Wcislo, S. Yu, E. Zak, The HITRAN2016 molecular spectroscopic database, *J. Quant. Spectrosc. Radiat. Transfer*. doi: 10.1016/j.jqsrt.2017.06.038.
- [2] L.S. Rothman, I.E. Gordon, Y. Babikov, A. Barbe, D. Chris Benner, P.F. Bernath, M. Birk, L. Bizzocchi, V. Boudon, L.R. Brown, A. Campargue, K. Chance, E.A. Cohen, L.H. Coudert, V.M. Devi, B.J. Drouin, A. Fayt, J.M. Flaud, R.R. Gamache, J.J. Harrison, J.M. Hartmann, C. Hill, J.T. Hodges, D. Jacquemart, A. Jolly, J. Lamouroux, R.J. Le Roy, G. Li, D.A. Long, O.M. Lyulin, C.J. Mackie, S.T. Massie, S. Mikhailenko, H.S.P. Müller, O.V. Naumenko, A.V. Nikitin, J. Orphal, V. Perevalov, A. Perrin, E.R. Polovtseva, C. Richard, M.A.H. Smith, E. Starikova, K. Sung, S. Tashkun, J. Tennyson, G.C. Toon, V.G. Tyuterev, G. Wagner, The HITRAN2012 molecular spectroscopic database, *J. Quant. Spectrosc. Radiat. Transfer* 130 (2013) 4–50.
- [3] N. Jacquinet-Husson, R. Armante, N.A. Scott, A. Chédin, L. Crépeau, C. Boutammine, A. Bouhdaoui, C. Crevoisier, V. Capelle, C. Boone, N. Poulet-Crovisier, A. Barbe, D. Chris Benner, V. Boudon, L.R. Brown, J. Buldyreva, A. Campargue, L.H. Coudert, V.M. Devi, M.J. Down, B.J. Drouin, A. Fayt, C. Fittschen, J.M. Flaud, R.R. Gamache, J.J. Harrison, C. Hill, Ø. Hodnebrog, S.M. Hu, D. Jacquemart, A. Jolly, E. Jiménez, N.N. Lavrenteva, A.W. Liu, L. Lodi, O.M. Lyulin, S.T. Massie, S. Mikhailenko, H.S.P. Müller, O.V. Naumenko, A. Nikitin, C.J. Nielsen, J. Orphal, V.I. Perevalov, A. Perrin, E. Polovtseva, A. Predoi-Cross, M. Rotger, A.A. Ruth, S.S. Yu, K. Sung, S.A. Tashkun, J. Tennyson, V.G. Tyuterev, J. Vander Auwera, B.A. Voronin, A. Makie, The 2015 edition of the GEISA spectroscopic database, *J. Mol. Spectrosc.* 327 (2016) 31–72.
- [4] I.E. Gordon, L.S. Rothman, R.R. Gamache, D. Jacquemart, C. Boone, P.F. Bernath, M. Shephard, J.S. Delamere, S.A. Clough, Current updates of water vapor linelist in HITRAN2004: a new "Diet" for air-broadened half-widths, *J. Quant. Spectrosc. Radiat. Transfer* 108 (2007) 389–402.
- [5] G.L. Villanueva, M.J. Mumma, B.P. Bonev, R.E. Novak, R.J. Barber, M.A. DiSanti, Water in planetary and cometary atmospheres: $\text{H}_2\text{O}/\text{HDO}$ transmittance and fluorescence models, *J. Quant. Spectrosc. Radiat. Transfer* 113 (2012) 202–220.
- [6] R.J. Barber, J. Tennyson, G.J. Harris, R.N. Tolchenov, A high-accuracy computed water line list, *Mon. Not. R. Astron. Soc.* 368 (2006) 1087–1094.
- [7] J.Y. Mandin, C. Camy-Peyret, J.M. Flaud, G. Guelachvili, Measurements and calculations of self-broadening coefficients of lines belonging to the $2\nu_2$, ν_1 and ν_3 bands of H_2^{16}O , *Can. J. Phys.* 60 (1982) 94–101.
- [8] V.M. Devi, D.C. Benner, M.A.H. Smith, C.P. Rinsland, Measurements of pressure broadening and pressure shifting by nitrogen in the ν_1 and ν_3 bands of H_2^{16}O , *J. Mol. Spectrosc.* 155 (1992) 333–342.
- [9] R.A. Toth, $2\nu_2$ – ν_2 and $2\nu_2$ bands of H_2^{16}O , H_2^{17}O , and H_2^{18}O : line positions and strengths, *J. Opt. Soc. Am. B* 10 (1993) 1526–1544.

- [10] R.A. Toth, Measurements of positions, strengths and self-broadened widths of H₂O from 2900 to 8000 cm⁻¹: line strength analysis of the 2nd triad bands, *J. Quant. Spectrosc. Radiat. Transfer* 94 (2005) 51–107.
- [11] R.A. Toth, L.R. Brown, C. Plymate, Self-broadened widths and frequency shifts of water vapor lines between 590 and 2400 cm⁻¹, *J. Quant. Spectrosc. Radiat. Transfer* 59 (1998) 529–562.
- [12] R.A. Toth, Air- and N₂-broadening parameters of water vapor: 604 to 2271 cm⁻¹, *J. Mol. Spectrosc.* 201 (2000) 218–243.
- [13] L.R. Brown, R.A. Toth, M. Dulick, Empirical line parameters of H₂¹⁶O near 0.94 μm: positions, intensities and air-broadening coefficients, *J. Mol. Spectrosc.* 212 (2002) 57–82.
- [14] A. Bruno, G. Pesce, G. Rusciano, A. Sasso, Self-, nitrogen-, and oxygen-broadening coefficient measurements in the ν₁ band of H₂O using a difference frequency generation spectrometer at 3 μm, *J. Mol. Spectrosc.* 215 (2002) 244–250.
- [15] Q. Zou, P. Varanasi, Laboratory measurement of the spectroscopic line parameters of water vapor in the 610–2100 and 3000–4050 cm⁻¹ regions at lower-tropospheric temperatures, *J. Quant. Spectrosc. Radiat. Transfer* 82 (2003) 45–98.
- [16] D. Lisak, G. Rusciano, A. Sasso, An accurate comparison of lineshape models on H₂O lines in the spectral region around 3μm, *J. Mol. Spectrosc.* 227 (2004) 162–171.
- [17] R.A. Toth, Measurements and analysis (using empirical functions for widths) of air- and self-broadening parameters of H₂O, *J. Quant. Spectrosc. Radiat. Transfer* 94 (2005) 1–50.
- [18] D. Jacquemart, R. Gamache, L.S. Rothman, Semi-empirical calculation of air-broadened half-widths and air pressure-induced frequency shifts of water-vapor absorption lines, *J. Quant. Spectrosc. Radiat. Transfer* 96 (2005) 205–239.
- [19] L.R. Brown, D. Chris Benner, V. Malathy Devi, M.A.H. Smith, R.A. Toth, Line mixing in self- and foreign-broadened water vapor at 6 μm, *J. Mol. Struct.* 742 (2005) 111–122.
- [20] G. Wagner, M. Birk, R.R. Gamache, J.-M. Hartmann, Collisional parameters of H₂O lines: effects of temperature, *J. Quant. Spectrosc. Radiat. Transfer* 92 (2005) 211–230.
- [21] R.A. Toth, L.R. Brown, M.A.H. Smith, V. Malathy Devi, D.C. Benner, M. Dulick, Air-broadening of H₂O as a function of temperature: 696–2163 cm⁻¹, *J. Quant. Spectrosc. Radiat. Transfer* 101 (2006) 339–366.
- [22] H. Tran, D. Bermejo, J.-L. Domenech, P. Joubert, R.R. Gamache, J.-M. Hartmann, Collisional parameters of H₂O lines: velocity effects on the line shape, *J. Quant. Spectrosc. Radiat. Transfer* 108 (2007) 126–145.
- [23] M. Birk, G. Wagner, Temperature-dependent air broadening of water in the 1250–1750 cm⁻¹ range, *J. Quant. Spectrosc. Radiat. Transfer* 113 (2012) 889–928.
- [24] C.S. Goldenstein, R.K. Hanson, Diode-laser measurements of linestrength and temperature-dependent lineshape parameters for H₂O transitions near 1.4 μm using Voigt, Rautian, Galatry, and speed-dependent Voigt profiles, *J. Quant. Spectrosc. Radiat. Transfer* 152 (2015) 127–139.
- [25] M. Birk, G. Wagner, Voigt profile introduces optical depth dependent systematic errors – detected in high resolution laboratory spectra of water, *J. Quant. Spectrosc. Radiat. Transfer* 170 (2016) 159–168.
- [26] I.V. Ptashnik, R. McPheat, O.L. Polyansky, K.P. Shine, K.M. Smith, Intensities and self-broadening coefficients of the strongest water vapour lines in the 2.7 and 6.25 μm absorption bands, *J. Quant. Spectrosc. Radiat. Transfer* 177 (2016) 92–107.
- [27] J. Loos, M. Birk, G. Wagner, Measurement of air-broadening line shape parameters and temperature dependence parameters of H₂O lines in the spectral ranges 1850–2280 cm⁻¹ and 2390–4000 cm⁻¹, *J. Quant. Spectrosc. Radiat. Transfer* 203 (2017) 103–118.
- [28] J. Loos, M. Birk, G. Wagner, Measurement of positions, intensities and self-broadening line shape parameters of H₂O lines in the spectral ranges 1850–2280 cm⁻¹ and 2390–4000 cm⁻¹, *J. Quant. Spectrosc. Radiat. Transfer* 203 (2017) 119–132.
- [29] R.R. Gamache, J. Fischer, Half-widths of H₂¹⁶O, H₂¹⁸O, H₂¹⁷O, HD¹⁶O, and D₂¹⁶O: II Comparison with Measurements, *J. Quant. Spectrosc. Radiat. Transfer* 78 (2003) 305–318.
- [30] R.R. Gamache, J. Fischer, Half-widths of H₂¹⁶O, H₂¹⁸O, H₂¹⁷O, HD¹⁶O, and D₂¹⁶O: I Comparison between Isotopomers, *J. Quant. Spectrosc. Radiat. Transfer* 78 (2003) 289–304.
- [31] R.R. Gamache, J.-M. Hartmann, An intercomparison of measured pressure-broadening and pressure-shifting parameters of water vapor, *Can. J. Chem.* 82 (2004) 1013–1027.
- [32] R.R. Gamache, J.-M. Hartmann, Collisional parameters of H₂O lines: effects of vibration, *J. Quant. Spectrosc. Radiat. Transfer* 83 (2004) 119–147.
- [33] R.R. Gamache, Line Shape parameters for water vapor in the 3.2 to 17.76 μm region for Atmospheric Applications, *J. Mol. Spectrosc.* 229 (2005) 9–18.
- [34] B.K. Antony, R. Gamache, Self-broadened half-widths and self-induced line shifts for water vapor transitions in the 3.2–17.76 μm spectral region via complex Robert-Bonamy theory, *J. Mol. Spectrosc.* 243 (2007) 113–123.
- [35] R.R. Gamache, A.L. Laraia, N₂-, O₂-, and air-broadened half-widths, their temperature dependence, and line shifts for the rotation band of H₂¹⁶O, *J. Mol. Spectrosc.* 257 (2009) 116–127.
- [36] L.R. Brown, K. Sung, D.C. Benner, V.M. Devi, V. Boudon, T. Gabard, C. Wenger, A. Campargue, O. Leshchishina, S. Kassi, D. Mondelain, L. Wang, L. Daumont, L. Régalia, M. Rey, X. Thomas, V.G. Tyuterev, O.M. Lyulin, A.V. Nikitin, H.M. Niederer, S. Albert, S. Bauerecker, M. Quack, J.J. O'Brien, I.E. Gordon, L.S. Rothman, H. Sasada, A. Coustenis, M.A.H. Smith, T. Carrington, X.G. Wang, A.W. Mantz, P.T. Spickler, Methane line parameters in the HITRAN2012 database, *J. Quant. Spectrosc. Radiat. Transfer* 130 (2013) 201–219.
- [37] V. Malathy Devi, D.C. Benner, M.A.H. Smith, C.P. Rinsland, S.W. Sharpe, R.L. Sams, A multispectrum analysis of the ν₁ band of H¹²C¹⁴N: Part I Intensities, self-broadening and self-shift coefficients, *J. Quant. Spectrosc. Radiat. Transfer* 82 (2003) 319–341.
- [38] C.P. Rinsland, V. Malathy Devi, M.A.H. Smith, D. Chris Benner, S.W. Sharpe, R.L. Sams, A multispectrum analysis of the ν₁ band of H¹²C¹⁴N: Part II. Air- and N₂-broadening, shifts and their temperature dependences, *J. Quant. Spectrosc. Radiat. Transfer* 82 (2003) 343–362.
- [39] A.G. Maki, J.S. Wells, Wavenumber Calibration Tables from Heterodyne Frequency Measurements (version 1.3), National Institute of Standards and Technology, Gaithersburg, MD, 2017.
- [40] D.C. Benner, C.P. Rinsland, V.M. Devi, M.A.H. Smith, D. Atkins, A multispectrum nonlinear least squares fitting technique, *J. Quant. Spectrosc. Radiat. Transfer* 53 (1995) 705–721.
- [41] K.L. Letchworth, D.C. Benner, Rapid and accurate calculation of the Voigt function, *J. Quant. Spectrosc. Radiat. Transfer* 107 (2007) 173–192.
- [42] A. Levy, N. Lacombe, C. Chackerian Jr. (Eds.), Collisional Line Mixing, in *Spectroscopy of the Earth's Atmosphere and Interstellar Medium*, Academic Press, Inc., Boston, 1992, pp. 261–337.
- [43] A. Vitcu, Line Shape Studies in the 0310–01101 Q Branch of N₂O Using a Mid-Infrared Difference-Frequency Spectrometer, University of Toronto, Canada, Ph.D., 2003.
- [44] V.M. Devi, D.C. Benner, K. Sung, T.J. Crawford, R.R. Gamache, C.L. Renaud, M.A. H. Smith, A.W. Mantz, G.L. Villanueva, Line parameters for CO₂ broadening in the ν₂ band of HD¹⁶O, *J. Quant. Spectrosc. Radiat. Transfer* 187 (2017) 472–488.
- [45] V.M. Devi, D.C. Benner, K. Sung, T.J. Crawford, R.R. Gamache, C.L. Renaud, M.A. H. Smith, A.W. Mantz, G.L. Villanueva, Line parameters for CO₂- and self-broadening in the ν₁ band of HD¹⁶O, *J. Quant. Spectrosc. Radiat. Transfer* 203 (2017) 133–157, <https://doi.org/10.1016/j.jqsrt.2017.01.032>.
- [46] V.M. Devi, D.C. Benner, K. Sung, T.J. Crawford, R.R. Gamache, C.L. Renaud, M.A. H. Smith, A.W. Mantz, G.L. Villanueva, Line parameters for CO₂- and self-broadening in the ν₃ band of HD¹⁶O, *J. Quant. Spectrosc. Radiat. Transfer* (2017), <https://doi.org/10.1016/j.jqsrt.2017.02.02s0> (in press).
- [47] P.W. Rosenkranz, Shape of the 5 mm oxygen band in the atmosphere, *IEEE Trans. Antennas Propag.* AP-23 (1975) 498–506.
- [48] M.A.H. Smith, D.C. Benner, A. Predoi-Cross, V.M. Devi, Multispectrum analysis of ¹²CH₄ in the ν₄ band: I. Air-broadened halfwidths, pressure-induced shifts, temperature dependences and line mixing, *J. Quant. Spectrosc. Radiat. Transfer* 110 (2009) 639–653.
- [49] H. Tran, P.-M. Flaud, T. Gabard, F. Hase, Clarmann Tv, C. Camy-Peyret, S. Payan, J.-M. Hartmann, Model, software and database for line-mixing effects in the ν₃ and ν₄ bands of CH₄ and tests using laboratory and planetary measurements—I: N₂ (and air) broadenings and the earth atmosphere, *J. Quant. Spectrosc. and Radiat. Transfer* 101 (2006) 284–305.
- [50] D. Robert, J. Bonamy, Short range force effects in semiclassical molecular line broadening calculations, *J. Phys. France* 40 (1979) 923–943.
- [51] Q. Ma, R.H. Tipping, C. Boulet, Modification of the Robert-Bonamy formalism in calculating Lorentzian half-widths and shifts, *J. Quant. Spectrosc. Radiat. Transfer* 103 (2007) 588–596.
- [52] J.E. Jones, On the determination of molecular fields. II. From the equation of state of a gas, *Proc. R. Soc. A* 106 (1924) 463–477.
- [53] J.O. Hirschfelder, C.F. Curtiss, R.B. Bird, *Molecular Theory of Gases and Liquids*, Wiley, New York, 1964.
- [54] R.A. Sack, Two-center expansion for the powers of the distance between two points, *J. Math. Phys.* 5 (1964) 260–268.
- [55] R.R. Gamache, L. Rosenmann, The effects of velocity averaging in broadening coefficient calculations, *J. Mol. Spectrosc.* 164 (1994) 489–499.
- [56] R. Lynch, R.R. Gamache, S.P. Neshyba, Fully complex implementation of the Robert-Bonamy formalism: half widths and line shifts of H₂O broadened by N₂, *J. Chem. Phys.* 105 (1996) 5711–5721.
- [57] R.R. Gamache, Analytical evaluation of the Maxwell-Boltzmann velocity average in pressure-broadened half-width calculations, *J. Mol. Spectrosc.* 208 (2001) 79–86.
- [58] J. Lamouroux, R.R. Gamache, A.L. Laraia, J.-M. Hartmann, C. Boulet, Semiclassical calculations of half-widths and line shifts for transitions in the 30012–00001 and 30013–00001 bands of CO₂ II: collisions with O₂ and Air, *J. Quant. Spectrosc. Radiat. Transfer* 113 (2012) 991–1003.
- [59] L. Rosenmann, J.-M. Hartmann, M.Y. Perrin, J. Taine, Collisional broadening of CO₂ IR lines. II. Calculations, *J. Chem. Phys.* 88 (1988) 2999–3006.
- [60] J.-P. Bouanich, Site-site Lennard-Jones potential parameters for N₂, O₂, H₂, CO and CO₂, *J. Quant. Spectrosc. Radiat. Transfer* 47 (1992) 243–250.
- [61] D. Lambot, A. Olivier, G. Blanquet, J. Walrand, J.P. Bouanich, Diode-laser measurements of collisional line broadening in the ν₅ band of C₂H₂, *J. Quant. Spectrosc. Radiat. Transfer* 45 (1991) 145–155.
- [62] M. Diaz Pena, C. Pando, J.A.R. Renuncio, Combination rules for intermolecular potential parameters. I. Rules based on approximations for the long-range dispersion energy, *J. Chem. Phys.* 76 (1982) 325–332.
- [63] M. Diaz Pena, C. Pando, J.A.R. Renuncio, Combination rules for intermolecular potential parameters. II. Rules based on approximations for the long-range dispersion energy and an atomic distortion model for the repulsive interactions, *J. Chem. Phys.* 76 (1982) 333–339.

- [64] R.J. Good, C.J. Hope, Test of combining rules for intermolecular distances. Potential function constants from second virial coefficients, *J. Chem. Phys.* 55 (1971) 111–116.
- [65] J. Lamouroux, R.R. Gamache, A.L. Laraia, Q. Ma, R.H. Tipping, Comparison of trajectory models in calculations of N_2 -broadened half-widths and N_2 -induced line shifts for the rotational band of $H_2^{16}O$ and comparison with measurements, *J. Quant. Spectrosc. Radiat. Transfer* 113 (2012) 951–960.
- [66] J.-M. Hartmann, J. Taine, J. Bonamy, B. Labani, D. Robert, Collisional broadening of rotation–vibration lines for asymmetric-top molecules II. H_2O diode laser measurements in the 400–900 K range; calculations in the 300–2000 K range, *J. Chem. Phys.* 86 (1987) 144–156.
- [67] A. Predoi-Cross, A.R.W. McKellar, D.C. Benner, V.M. Devi, R.R. Gamache, C.E. Miller, R.A. Toth, L.R. Brown, Temperature dependences for air-broadened Lorentz half-width and pressure shift coefficients in the 30013–00001 and 30012–00001 bands of CO_2 near 1600 nm, *Can J. Phys.* 87 (2009) 517–535.
- [68] N.H. Ngo, D. Lisak, H. Tran, J.M. Hartmann, An isolated line-shape model to go beyond the Voigt profile in spectroscopic databases and radiative transfer codes, *J. Quant. Spectrosc. Radiat. Transfer* 129 (2013) 89–100, Erratum. *J. Quant. Spectrosc. Radiat. Transf.* 134 (2014) 105.
- [69] N.H. Ngo, D. Lisak, H. Tran, J.M. Hartmann, Erratum to “An isolated line-shape model to go beyond the Voigt profile in spectroscopic databases and radiative transfer codes” [*J. Quant. Spectrosc. Radiat. Transf.* 129, 89–100], *J. Quant. Spectrosc. Radiat. Transfer* 2014 (134) (2013) 105.
- [70] H. Tran, N.H. Ngo, J.M. Hartmann, Efficient computation of some speed-dependent isolated line profiles, *J. Quant. Spectrosc. Radiat. Transfer* 129 (2013) 199–203, Erratum. *J. Quant. Spectrosc. Radiat. Transf.* 134 (2014) 04.
- [71] H. Tran, N.H. Ngo, J.M. Hartmann, Erratum to “Efficient computation of some speed-dependent isolated line profiles” [*J. Quant. Spectrosc. Radiat. Transfer* 129, 199–203], *J. Quant. Spectrosc. Radiat. Transfer* 2014 (134) (2013) 104.